ELECTRICAL POWER GENERATION FROM NON-CONTINUOUS FLOW IN A SELF-CONTAINED BREATHING APPARATUS

by

Matthew James Palamara

BS, Pennsylvania State University, 2002

Submitted to the Graduate Faculty of

School of Engineering in partial fulfillment

of the requirements for the degree of

Master of Science Mechanical Engineering

University of Pittsburgh

2004

UNIVERSITY OF PITTSBURGH

SCHOOL OF ENGINEERING

This thesis was presented

by

Matthew James Palamara

It was defended on

April 6th, 2004

and approved by

Dr. Michael R. Lovell, Associate Dean for Research

Dr. Marlin H. Mickle, Professor, Electrical Engineering Dept.

Thesis Advisor: Dr. Roy D. Marangoni, Associate Professor, Mechanical Engineering Dept.

ELECTRICAL POWER GENERATION FROM NON-CONTINUOUS FLOW IN A SELF-CONTAINED BREATHING APPARATUS

Matthew J. Palamara, B.S.

University of Pittsburgh, 2004

In recent times, the number of electronic devices utilized by firefighters has greatly increased. Currently, all of this equipment relies heavily upon batteries as a source of power. The purpose of this research was to investigate alternate methods for powering the electrical functions of an SCBA (self-contained breathing apparatus). Replacing the batteries with a self-sufficient source of constant power is attractive for its characteristics of both reliability and cost efficiency. Maintenance of charged batteries and the logistics problem of an SCBA arriving at the scene unable to operate create an environment which is certainly unreliable and potentially quite dangerous. By relying on a maintenance-free, constant source of power, the jobs of fire departments could be made easier, and the lives of firefighters safer.

The energy source for the power generation was to be the pressurized air stored in tanks on the firefighters' backs. Many methods were considered for the ground-up design, but selected was the concept of an inline unit comprised of a small DC dynamo coupled with a pneumatic motor. The generator would be propelled by the air flow resulting from each inhalation breath. Multiple tests were performed to prove the generator's capability in both adequate continuous power generation and in its implementation without affecting the existing performance of the SCBA. An accumulator was added to the system as a corrective method to keep the internal mask pressure at an acceptable level.

The final design of the power generation cell includes a non-reversible air motor, coupled with the appropriate DC motor, contained within a sealed cell which acts as an accumulator, protective enclosure, and a means of leak containment for the unit. The unit is self-contained,

easily added to an SCBA, and has no negative effects on the current design of the system. Adequate levels of continuous power were reached, ranging from 4 to 7 Watts depending on the rate of breathing.

TABLE OF CONTENTS

LIST OF TABLES

LIST OF FIGURES

ACKNOWLEDGEMENTS

First, I would like to thank Mine Safety Appliances, Inc. and the University of Pittsburgh for supplying me with the funding and equipment necessary to make this project a successful one. I would like to thank Dr. Roy Marangoni, my academic and thesis advisor, for all of his continued support and guidance throughout my research and studies at the University of Pittsburgh. Next, I would like to thank Jim Hendrickson from MSA for all of his creative and time-consuming contributions, as well as the continuous positive outlook that he brought to this project. Additionally, I thank the following MSA employees, without whom my research could not have taken place: Rick Katz, John Kuhn, John Mulcahy, Mike Theodore, Jim Tudor, Ray Milliren, Bill Anderson, Steve Hanechek, and Rich Kline. I would also like to thank Dr. Mike Lovell and Dr. Marlin Mickle for overseeing my thesis defense. Finally, I would like to thank my family, the best there is, and God, the One who has brought me this far.

1.0 INTRODUCTION

1.1 PROJECT DESCRIPTION

In short, the purpose of this research was to investigate alternate methods for powering the electrical functions of an SCBA and its related devices. The power production method would act as a replacement or supplement of the batteries that now power the system's components. Safety devices, head-up displays, communications devices, and thermal imaging cameras are all currently utilized by modern firefighters, and were all to be considered when accounting for power consumption. The following is a list of estimated power consumptions that describes the power required for the support of this equipment:

HUD (Head-Up-Display): 0.25 W

PASS (Personal Alert Safety System): 1.00 W

TIC (Thermal Imaging Camera): 5 W

A photograph of a typical SCBA unit is shown in Fig. (1.1) below. Important components are pointed out, including the pressurized air cylinder and both first and second-stage regulators.

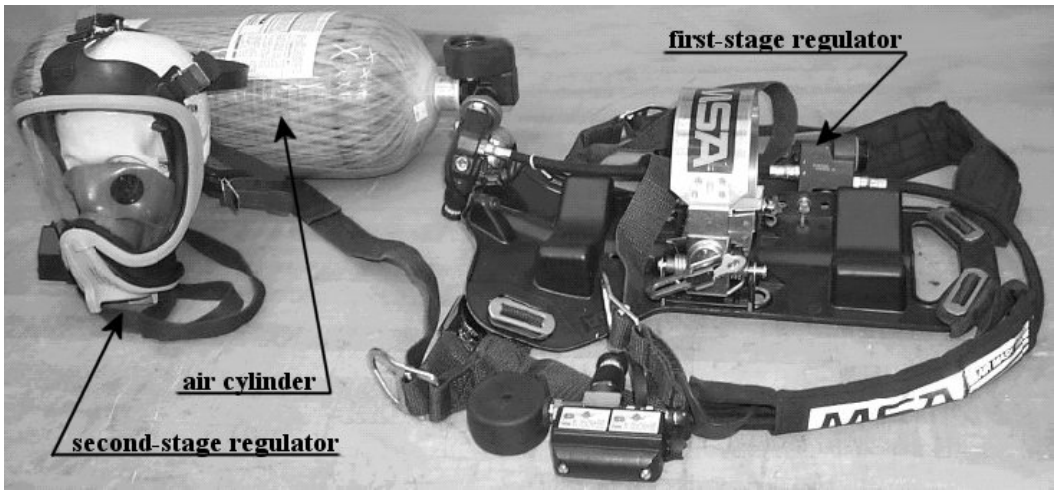

Figure 1.1: Components of the Self-Contained Breathing Apparatus

The current arrangement of the SCBA's components begins with a large cylinder of pressurized air (generally 2216 psi) which is typically mounted on a backpack worn by the firefighter (shown removed from the backpack). Breathing air flows through a high-pressure hose from the cylinder into a first-stage pressure regulator. This pressure regulator is comprised of a metal casing which channels the pressurized air into a spring-valve arrangement with a specified spring stiffness where the air is then released into a small chamber. At this point, the pressure has been reduced to between 80 and 100 psi. The air then flows through another hose into a second-stage regulator, attached to the facemask being worn by the firefighter. (Note: In Fig. (1.1), the second hose is not attached to the second-stage regulator on the facemask). It is in the dynamic, mechanical system of the second-stage regulator that the air is brought to a pressure slightly (1 or 2 inches of water) above atmospheric for the firefighter to breath inside the mask. It should be noted that it is crucial that the mask pressure remain above atmospheric at all times so that in the event of dislodging, air will flow outward instead of drawing potentially deadly gases and fumes into the breathing mask.

It was estimated through calculations that the potential power stored in the pressurized cylinder of air was certainly enough to warrant further research of power production capability. The depressurization of the air cylinder was considered, and the Ideal Gas Law was assumed [1]:

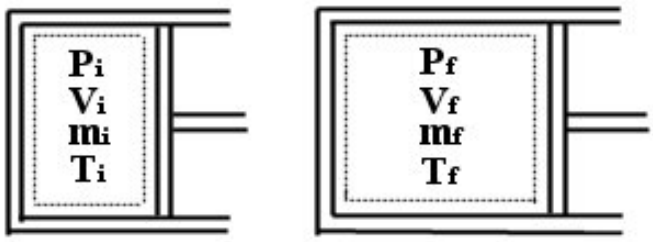

$Ti = Tf = T$ (assume slow expansion)

$mi = mf = m$ (assume closed system)

Ideal Gas Law: $P \cdot V = m \cdot R \cdot T$ reduces to…

$$W = -Pi \cdot Vi \cdot \ln\left[\frac{Pf}{Pi}\right] \tag{1.1}$$

…where W is the power produced in Watts (assuming a 30 minute flow time), Pi is the initial pressure in the air cylinder, Vi is the initial volume of the cylinder, and Pf is the final pressure. Inserting these values into the above equation, the potential power is given as $W = 354$ Watts. Of this amount, however, only about 131 Watts remains available for power extraction downstream of the first-stage regulator. This value was calculated in the same way as above, only this time subtracting the power wasted by the first-stage regulator in dropping the pressure to 80 psi. Altogether, this study helped prove the feasibility of the power generation project.

For reasons discussed later in this report, it was in fact determined that a location between the first and second-stage regulators was the best place to tap into the system for power production. Replacement of the first-stage regulator with a power producing unit which also acted as a pressure regulator was considered an option, as well as the less desirable redesign of

the second-stage regulator. The foremost problem with this idea, however, was that the components of the power producing unit would have to withstand the typical 2216 psi pressure stored in the cylinder. It was also required that size, weight, and integration of the power generation system would not have any significant adverse effect on the function, storage, or maintenance of the SCBA. Additionally, the power generation system was not to exceed a targeted $200 incremental increase to the current SCBA manufacturing cost.

1.2 ELECTRICAL POWER GENERATION

Electrical power generation has been a subject of research in the field of engineering for well over a hundred years. Several methods for this generation are as follows: static electricity, photo electricity, thermoelectricity, electrochemistry, piezoelectric effects, and magnetic induction.

Aside from its recent applications in micro-machines and integrated circuits, electrostatic power generation has been deemed inefficient in comparison with other like methods because of its high voltage requirements and weak performance. Photoelectric, or solar power, and thermoelectric power are not viable options for SCBA power generation needs because of their dependence on light and heat sources, respectively – two things to which firefighters are not guaranteed exposure.

Electrochemistry utilizes a chemical reaction between two substances (usually a chemical and a metal) which produces an exchange of electrons and, consequently, voltage. This is the method of power production, existing in the form of batteries, which has been previously used by firefighters to operate the electrical functions associated with an SCBA. The problem with this method of generating power is that electrochemistry is generally limited to the supplied amount

of reactants used in the process. In other words, it is not a continuous form of power generation, as is apparent through the frequent need for battery replacement.

Certainly one of the electrochemical devices with the most potential for such a project is the fuel cell. A fuel cell can most simply be described as a complex electrochemical device that converts hydrogen and oxygen into water while producing both electricity and heat in the process. The fuel cell best suited for power generation is known as the proton exchange membrane fuel cell, or PEMFC. A diagram depicting the electrochemical process of energy conversion in a PEMFC is shown below in Fig. (1.2).

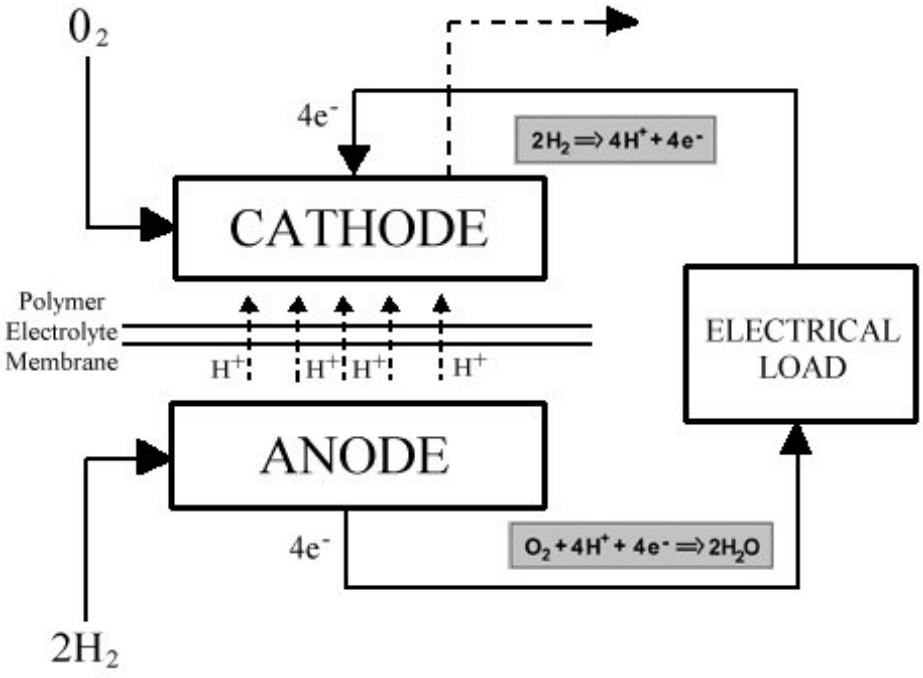

Figure 1.2: Proton Exchange Membrane Fuel Cell

A serious problem with this fuel cell being used in conjunction with the standard firefighter's apparatus rests in its reliance on the storage of a quite flammable fuel. The oxygen that the PEMFC uses in its electrochemical energy conversion process is typically not a problem, as it

can be drawn from air. Hydrogen, however, is an extremely flammable gas which can be hazardous to both handle and store, not to mention amidst the environment to which the aforementioned apparatus will be exposed. It is for reasons such as this that a device known as a reformer is often used to convert a more manageable type of fuel into hydrogen for use in the PEMFC. Even these less flammable fuels, however, often ranging from natural gas and propane to methanol, would be hazardous in an environment with extremely high levels of heat and open flames. Perhaps the most prominent disadvantage to current fuel cell technology is the price. Although there does exist some affordable, portable fuel cells, they are nothing more than containers of compressed, flammable, liquefied gas capable of only finite operation times before replacement is necessary.

Piezoelectricity is the ability of certain crystals to produce electrical energy when subjected to mechanical stress. Much research has been performed in the field of piezoelectric power generation and even its application of powering firefighters' equipment. Piezoelectric systems have been explored which use the pressure of the compressed air in a firefighter's breathing supply to stress a piezoelectric crystal, thus generating electrical power. A pressure activated, piezoelectric power generator [3,4] was developed by students at the University of Pittsburgh in which a piezoelectric film was adhered to a diaphragm positioned in the bottom of a pressure vessel. This apparatus was designed to be connected to the first-stage regulator of an SCBA such that upon an inhalation breath, the regulator would release the pressure in the vessel, causing the diaphragm to deflect and consequently generating a distinct voltage. Upon testing the generator under pressures of up to 25 psi, however, inadequate amounts of power were produced.

This example leads to the foremost disadvantage of using piezoelectricity as a method of generating electrical power for consumption - the very small amount of current which is created by the crystals. For this reason, the piezoelectric phenomenon is most commonly used for measurements and sensors, not power production.

Magnetic induction is the process of rotating a coil of wires through a stationary magnetic field, or vice versa. This method is widely used in large scale, commercial power generation systems today. Wind, water, or steam is often used as the exciting force to activate the process. This applied force (**F**) produces a current (***i***), the direction of which is such that the right-handed rotation of the current itself is consistent with the direction of the magnetic field lines (**B**) (Fig. (1.3)).

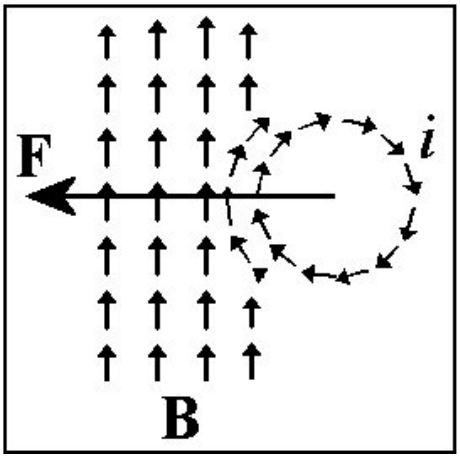

Figure 1.3: Magnetic Induction Theory

Typically, electric motors are operated based on the reverse of this theory, when an electric current in a magnetic field experiences a force which is often converted into rotational motion. By applying this rotational motion (or force) to the same motor from an alternate, exciting source, the rotating coil of wires inside the motor's magnetic field produces a current which can be captured in the form of electrical energy. Thus, the concept of using an electric motor in

reverse, through the introduction of a rotation force, proves a competent method of electrical power generation with the voltage produced reflecting the equation [5]:

$$V = NB\frac{A}{t - t_0} \tag{1.2}$$

where A is the area of the magnetic field which forms the flux in the coil, B is the magnetic field, t is the time in seconds, and N is the number of turns of the coil needed to produce a voltage V.

This particular method of power generation and distribution would very closely resemble that of an automobile's alternator. The alternator likewise uses magnetic induction theory, as it powers a central battery to which all necessary electronic components are wired. This concept would be considered quite acceptable for use in the application of firefighters' equipment because of the lack of maintenance involved in replacing batteries and the corresponding lowered risk of equipment failure in the field.

2.0 COMPONENT SELECTION AND PRODUCTION

2.1 CONVERSION OF AIR FLOW INTO POWER USING THE INDUCTION GENERATION METHOD

To encounter the task of converting the dynamic pulses of air flow associated with the human breathing cycle into a usable source of constant electrical power, there were two basic principles that needed attention. The first was transferring the flow of air into some mechanical motion, exploitable by the induction generation process. The second hurdle consisted of using magnetic induction to convert the mechanical energy into electrical.

At first, pre-manufactured items were considered that had the ability to perform both of these tasks were explored. Flow meters, although typically used for measurement purposes, were considered an option. These instruments already exist for purchase and typically capture the energy of the flowing air by the utilization of a turbine or paddle wheel. The great disadvantage to these instruments, however, is that flow meters are designed to produce only enough voltage needed to measure the velocity of the airflow (not as power generators). This voltage and power is typically very small and much lower than the power required. The airflow measurement is determined by the voltage frequency, not the voltage.

An alternate solution was conceived which employs pneumatic motors to produce mechanical power from a lower-pressure point in the system, such as that found between the first and second-stage regulators. Preliminary comparison of the worst case, average flow rate estimates for the breathing apparatus with manufacturer data on one particular air motor

suggested that this solution may in fact be quite feasible (several Watts of mechanical power might be produced). Identified as likely pitfalls with regard to the insertion of an off-the-shelf air motor were design mismatch in light of the low SCBA flow rate, difficulty in adapting to varying pulsations in the breathing cycle, and perturbation of the existing second-stage regulator which could cause disruption of the breathing cycle. Through extensive research on the internet and in various catalogues, an initial air motor was selected for trial. Airflow capabilities, allowable operating pressure range, weight, size, and reversibility (allowing for an inlet and outlet) were all considered in choosing the Micro Motors MMR-0700 air motor. Added benefits to the motor included its low maintenance and rather sanitary operation, as it is typically used in dental drilling applications. Information and manufacturer data for this motor can be found in Fig. (A.1-4).

Although mechanical power extraction at high pressures (upwards of 2000 psi) seemed to be unrealistic, impulse turbines (paddle-wheels) were investigated (See Fig. (B.1)) as a second option. Initial concerns for this type of design included both the challenge of adapting to the low flow rates associated with the human breathing cycle, as well as any attendant longevity implications for designs involving high rotational speeds. Also, it was concluded that the concept of a constant-flow system was unrealistic given the parameters for equipment change. (Redesign of the second-stage regulator was considered an unattractive option). It was therefore decided that the power generation system would most likely have to be adapted to the pulses of air created by the breathing cycle.

For either realistic case (pneumatic motor or flow-driven turbine) it was apparent that, to produce mechanical power, there still existed a need to convert the rotational, mechanical energy into an electrical power source. By this time, piezoelectric power generation had been

abandoned as it had been made apparent that such a method could never adequately supply the power needs envisioned as essential in prospective, centralized power-sourcing solutions, allowing most of the potential energy to go to waste. Also, the possibility of a more efficient allocation of power by modifications/replacements of existing electrical components was suggested to MSA for consideration.

The concept of using a small DC motor in reverse (as a generator) seemed like the best option for this conversion of energy. However, while the prospect of a small DC motor being used to generate power looked very hopeful, as with any design idea, there were certainly many questions to be considered (torque needed to turn the motor, placement of the motor in the system, design of the complete in-line unit, etc.).

Given the inputs of torque and rotational speed from either mechanical power generation option above, two examples of DC motors (with brushes) were ordered and studied for their efficiency in creating electrical power. The two motors are the Maxon A-max 32 (32 mm diameter, 20 Watt DC motor) and the Maxon RE 35 (35 mm diameter, 90 Watt DC motor). The manufacturer data for these motors can be found in Fig. (A.5-6). A testing fixture was manufactured to hold the Micro Motors MMR-0700 air motor in place and properly aligned with the Maxon RE35 90 Watt DC motor, and aluminum couplings were machined to connect the shafts of the motors. The following graph is the result of comparison testing between the two DC motors at various constant flow rates when driven by the Micro Motors MMR-0700 air motor:

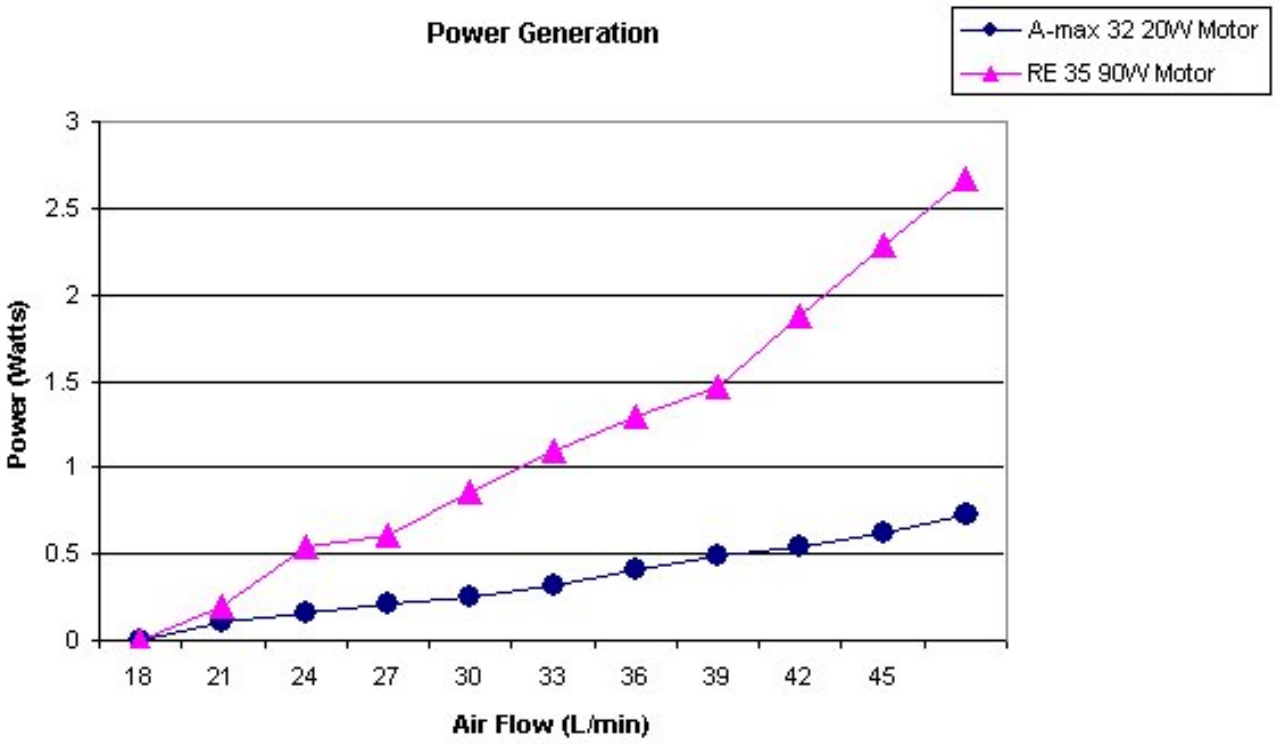

Figure 2.1: DC Motor Output Power Comparison (Pneumatic Motor Drive with Constant Flow)

Upon testing the DC motors together, it was made clear that the 90 Watt RE 35 motor would be a better choice for power production. The RE 35 consistently produced approximately three times the power as its counterpart rated at 20 Watts.

The power generation test assembly is pictured below in Fig. (2.2). Shown are both the DC and the pneumatic motors, the aluminum coupling, the alignment stand, and the pressure gauges.

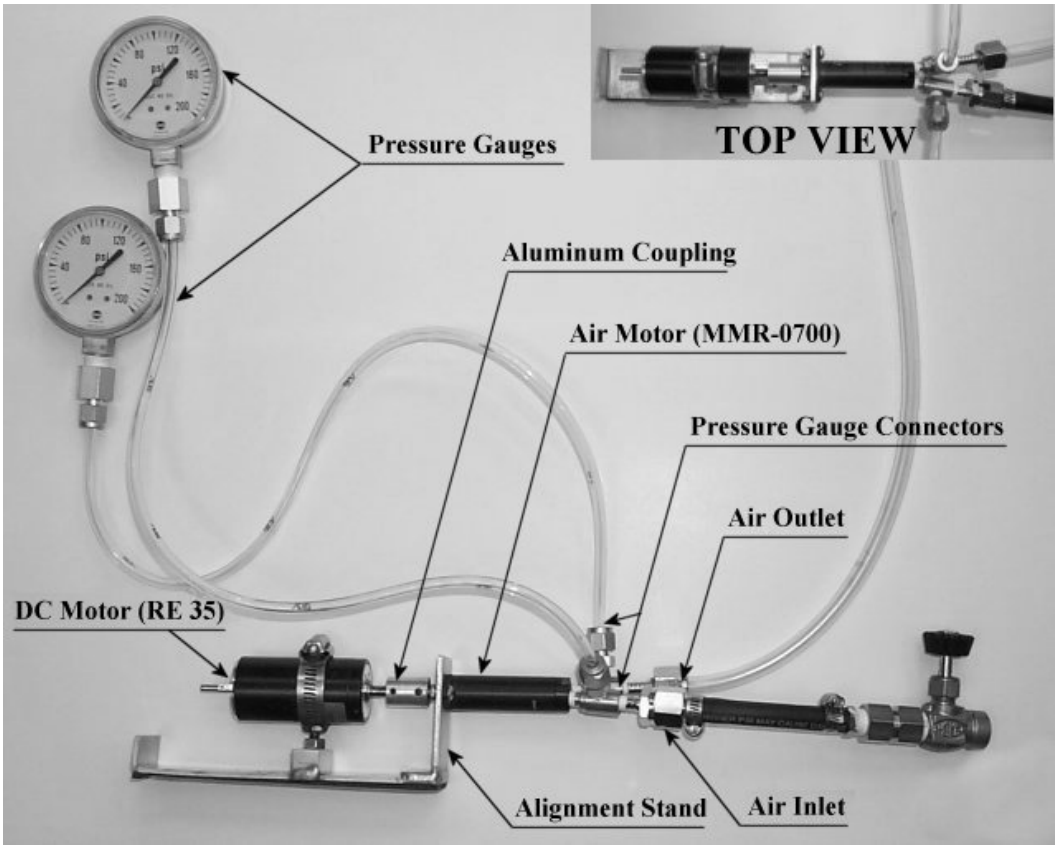

Figure 2.2: Power Generation Test Setup

Constant flow testing was first performed on the setup to better understand the power-generation capabilities of the system. These tests involved the use of "house air", which the system vented to atmosphere, and were performed in a lab at the University of Pittsburgh. The resistance values shown below refer to the circuit or load resistance to which the power is delivered. The following table of data was formed from the tests:

Table 2.1: Constant Flow Test Results - Maxon RE35 90 Watt DC Motor

FLOW		VOLTAGE	CURRENT	POWER
(SCFM)	(L/min)	(V)	(A)	(W)
1,000,000 Ω RESISTANCE				
0.5	14.2	42	4.00E-05	N/A
1.0	28.4	60	6.00E-05	N/A
1.5	42.5	1000+	7.00E-05	N/A
2.0	85.0	1000+	8.00E-05	N/A
1,000 Ω RESISTANCE				
0.5	14.2	40	4.09E-02	1.64
1.0	28.4	62	7.00E-02	4.34
120 Ω RESISTANCE				
0.5	14.2	22	0.200	4.40
1.0	28.4	33	0.276	9.11
1.5	42.5	40	0.330	13.20
10 Ω RESISTANCE				
0.5	14.2	3.6	0.375	1.35
1.0	28.4	5.5	0.570	3.14
1.5	42.5	7.0	0.750	5.25

The very positive results of the initial testing ceased research on the paddle-wheel turbine design and all resources were focused on the new pneumatic motor generation system. However, although the power output during a constant flow condition seemed adequate, further testing was needed to study the effectiveness of the new system in a more practical application. To do this, the apparatus was moved to the lab at Mine Safety Appliances, Inc. where it could be tested with their NIOSH (National Institute of Safety and Health) breathing simulation machine. The power generation system was connected in line with the SCBA between the first and second-stage regulators. This setup offered a much more realistic analysis of the power generating capabilities of the unit under pulsing, dynamic flow conditions similar to those associated with the human breathing cycle.

The breathing machine was set to the NIOSH “standard” work rate (40 L/min), its lowest setting, and an oscilloscope was used to monitor the dynamic nature of the power output. This

allowed us to capture the true power produced by the system over time. The following graph represents a freeze-frame of the power produced by the generator over one breathing cycle:

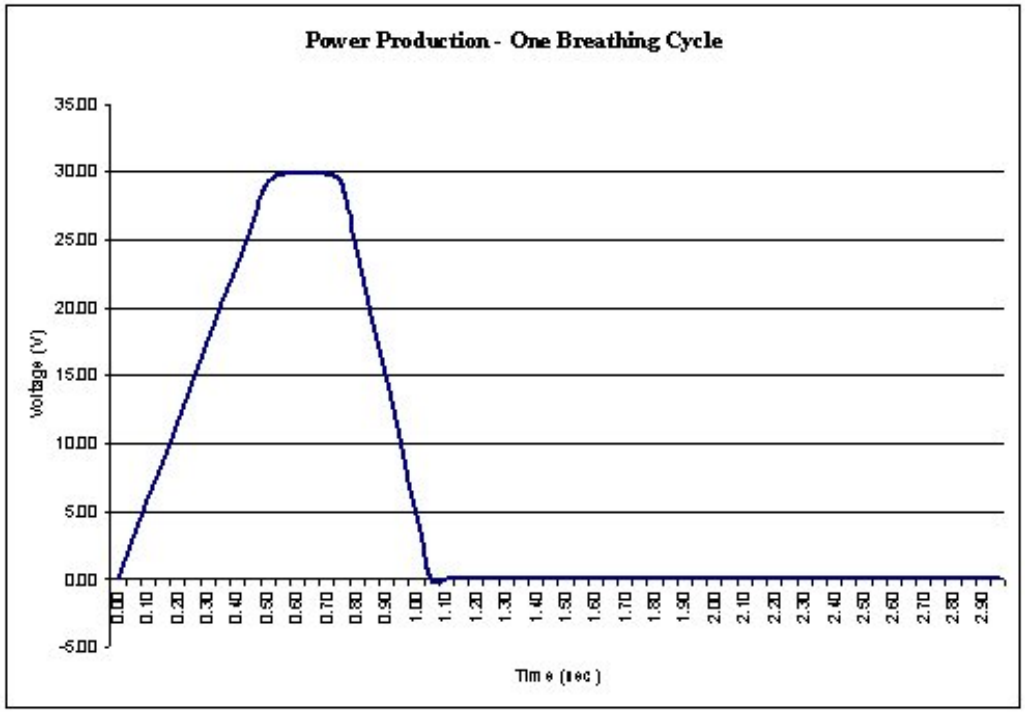

Figure 2.3: Electrical Power Production through One Breathing Cycle

The graph shown above was simplified (conservatively) into linear equations and integrated to estimate the "constant" power production of the generating system averaged over the entire breathing cycle. These equations are shown below:

$$V(t) = \left[\frac{30}{0.6}\right](t) \qquad (0 \le t \le 0.6) \tag{2.1}$$

$$V(t) = 60 - \left[\frac{30}{0.6}\right](t) \qquad (0.6 \le t \le 1.2) \tag{2.2}$$

Using $P(t) = \frac{V^2(t)}{R}$, the constant power production is…

$$\int_0^T P(t)\cdot d(t) = \frac{1}{R}\cdot\int_0^{0.6} 2500\cdot t^2\cdot dt + \frac{1}{R}\cdot\int_{0.6}^{1.2}(3600-6000\cdot t+2500\cdot t^2)\cdot dt \qquad (2.3)$$

Integrating this equation and using a time interval of T=2.95 seconds yields…

P=2.48 Watts

This is an acceptable power delivery; however, there remained issues that needed to be resolved.

One point of possible optimization of this output power involved adjusting the resistance that the DC generator is facing to the most efficient power-producing level for the system. A heavy-duty, variable resistor was connected to the circuit and the level of power generation was observed at different resistance loads. The following is a graph that depicts the changes in power output as a function of resistance while an arbitrary constant flow is maintained:

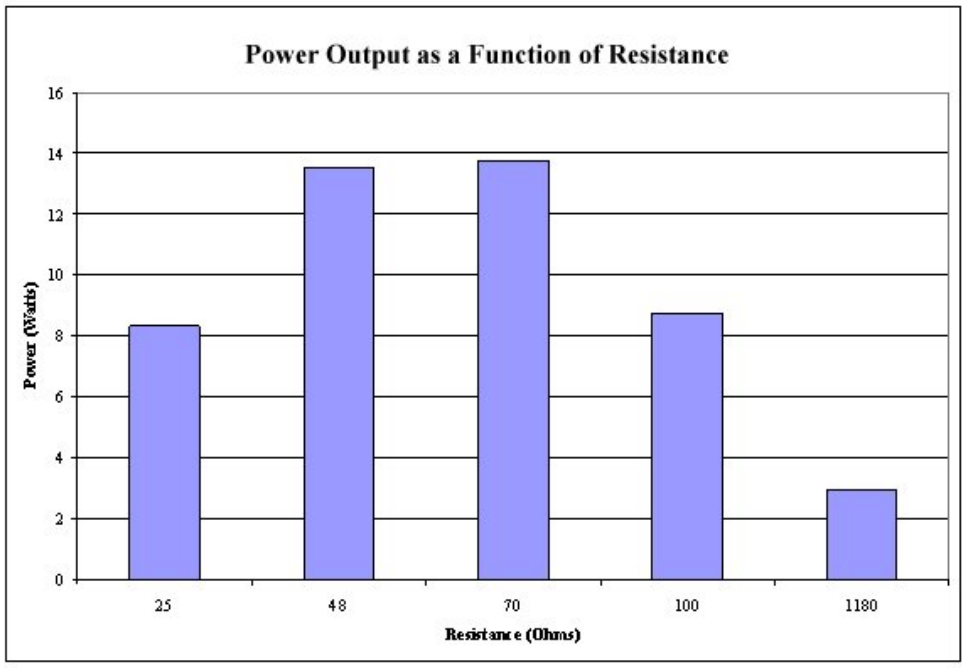

Figure 2.4: Power Output as a Function of Resistance

2.2 MASK AIR PRESSURE REGULATION

During the operation of the NIOSH breathing machine, it was observed that when the machine was adjusted to its “hard” work rate (maximum setting of approximately 100 L/min) the pressure inside the facemask became negative. As noted in Section 1.1, this is unacceptable, and options were later considered to correct the situation. The problem spawns from the fact that the second-stage regulator was built to accept air at an input pressure within a certain range. When the breathing machine is working the power generation system at the “hard” work rate, the pressure drop across the air motor becomes large enough to place the downstream pressure below the allowable range of the second-stage regulator’s input.

An initial consideration to resolve this condition was the idea of using an air motor with a greater (less restrictive) flow capacity so as to minimize the drop in pressure. After exhausting the internet as a resource for air motor research, the best higher-capacity pneumatic motor to meet the criteria was determined to be the ARO 8416-A (information found in Fig. (A.9-10). The current Micro Motors air motor only had a maximum flow capacity of 136 L/m while the new, larger ARO motor had a flow capacity of 324 L/m. It was doubtful, however, that there would prove much of a difference in pressure drop between the two motors because of the small capacity airlines and the dynamics of the first-stage regulator. When the Micro Motors air motor was switched with the new ARO motor, in fact, the results did not warrant a permanent replacement. The power delivery per flow rate was much lower on the new, bigger motor, and after sufficient testing it was determined that the Micro Motors air motor would be used.

The final and ultimately most attractive option to counter this issue of unacceptably low mask pressure was thought to be the placing of an air accumulator inline between the power generator and the second-stage regulator. Such a device could “cushion” the effects of the

dynamic system by storing enough air to supply the user with an entire breath. An accumulator would provide a pneumatic capacitance with the capability of decreasing the pressure loss across the generator to an acceptable level.

Experimentation was done to confirm this idea by lengthening the air hose in this area by a significant amount. The result of this quick adjustment was an increase in the pressure inside the facemask (although the increase still left the pressure below atmospheric). Also, it was not yet known how much such a change would reduce the power output of the generator. Fueled by these questions, an accumulator was designed for testing.

Important characteristics of an inline accumulator were determined to be the following: a variable volume, a means for simple and quick adjustment of volume, and reusability for extensive testing. With these specifications in mind, an accumulator was manufactured for placement downstream of the air motor. The accumulator consisted of a piece of 3-½ inch I.D., 1/4-inch thick aluminum pipe, machined to a length of 17 inches. Two 3/8 inch think, aluminum plates were cut to size and welded on the ends of the pipe. To accommodate the capability of an adjustable volume, the accumulator would be filled with water and then drained in increments, thus changing the amount of air in the accumulator, and as a result, its effect on the system. To provide for efficient operation, the accumulator was equipped with both a drain plug and a petcock on one end, while the inlet and outlet fittings were included on the opposite end.

The variable volume accumulator was placed inline between the outlet of the air motor and the inlet of the facemask. The facemask was attached to MSA's NIOSH breathing machine and multiple tests were run. The first test was done with an empty accumulator, and three more tests ensued decreasing the volume of the accumulator by 1/4 each time (1/4 volume = approximately 750 ml) with a final volume of 375 ml of water added to leave 1/8 of the

accumulator full of air. Finally, the system was also tested with no accumulator inline, for reference.

Because the initial testing was being done only to see if the accumulator would be sufficient in cushioning the pressure drop enough to maintain a positive mask pressure, the tests were all performed at the breathing machine's "hard" work rate (the maximum setting), which draws air at 100 L/min. This is the setting that had been causing the most problems with low mask pressure because of the massive pressure drop it forced across the air motor. An oscilloscope was used to measure the voltage output of the motor as the breathing machine propelled it. Images of the oscilloscope's screen were captured at each accumulator volume with a digital camera. These photographs are available in the Appendix (Fig. (B.2-4)). A chart, summarizing the findings of the incremental testing is shown below:

Table 2.2: Power Generation as a Function of Accumulator Volume

ACCUMULATOR VOLUME	VOLTAGE	CONSTANT POWER
(cm^3)	(V)	(W)
52 Ω RESISTANCE		
2837.9	10.6	2.16
2128.4	18.1	6.30
1418.9	19.4	7.23
709.4	17.5	5.90
354.7	20.0	7.70

Several trends could be noted from the experimentation done with the accumulator. First, the insertion of the accumulator in line allowed the mask pressure to remain above atmospheric pressure. With the accumulator at maximum volume (2837.9 cm^3 of air), the mask pressure was acting as if there was no power generation unit in the system at all, maintaining the expected

pressure of about 0.7-2.2 inches of water at all times. This remained almost completely consistent while decreasing its volume incrementally by the addition of water until the volume of 709.4 was reached. At this point, it was noted that the mask pressure began to drop slightly below atmospheric pressure at the beginning of the breathing machine's cycle then slowly rise back up above zero while the dynamic system reached a sort of equilibrium. The cause of this phenomenon was never completely determined, however it was obvious that this would be an unacceptable trend for mask pressure, therefore the recommendation size was backed to a 1418.9 cm^3 volume accumulator. A copy of some of the mask pressure results can be found in the Appendix (Fig. (B.5-6)).

Another obvious behavior could be noted about the power generation as the volume of the accumulator was slowly decreased. At the initial setting of a maximum volume accumulator, the DC and pneumatic motors surprisingly moved to a constantly spinning status. As the accumulator volume was decreased however, the "valleys" of the voltage graphs (Fig. (B.2-4)) clearly show that eventually the motor would stop spinning at its slowest points until the accumulator was full of water (no volume) and the graph would then be the same as the pulse graph shown previously in Fig. (2.3).

Now that the total system (power generator + accumulator) had been studied at the breathing machine's maximum flow rate, optimized for minimal allowable volume, and proven a success in fixing the problem of a unacceptably low mask pressure, it was considered desirable to re-test the system across the entire range of the breathing machines flow rates (standard, hard, and maximum) to gain a more broad picture of the power generation capability. This new experiment resulted in the flowing data:

Table 2.3: Power Generation at Various Flow Rates and Accumulator Volumes

FLOW RATE	ACCUMULATOR SIZE	VOLTAGE (RMS) OUT	CONSTANT POWER (W)
standard (~40 L/min)	2088 cm^3	3.20	0.20
hard	2088 cm^3	10.16	1.99
maximum (~100 L/min)	2088 cm^3	18.42	6.52
standard (~40 L/min)	**1338 cm^3**	**3.40**	**0.22**
hard	**1338 cm^3**	**10.43**	**2.09**
maximum (~100 L/min)	**1338 cm^3**	**20.19**	**7.84**
standard (~40 L/min)	588 cm^3	4.24	0.35
hard	588 cm^3	11.90	2.72
maximum (~100 L/min)	588 cm^3	21.44	8.84

NOTE: All tests performed used 52 ohms resistance.

The test indicated by the bold text above (with an accumulator size of 1338 cm^3) represents what was found to be the "best case" accumulator size tested. As can be seen, this is not the test that produced the most constant power, but as the accumulator size of 588 cm^3 was reached, the mask pressure results became undesirable. The following are graphs of the voltage output corresponding to the 1338 cm^3 accumulator volume. Both the standard and maximum work rates are shown.

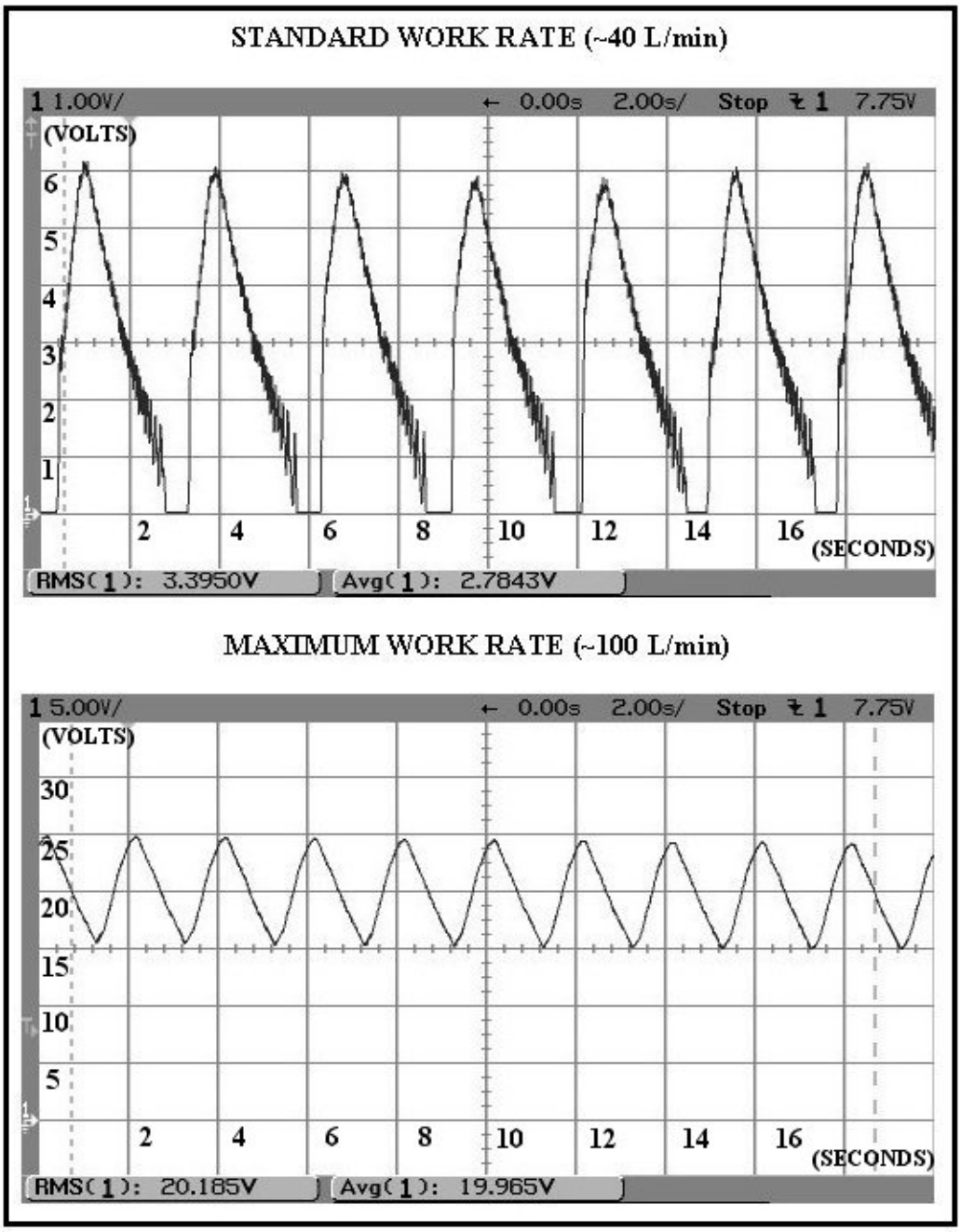

Figure 2.5: Generator Voltage Output Using 1338 cm^3 Accumulator

Overall, the second set of experimentation data (with the varying flow rates) displayed the same trends that were noted during the initial testing, and was likewise encouraging.

3.0 POWER CELL DESIGN AND TESTING

3.1 COMPONENT DESIGN AND ASSEMBLY

With regards to functionality, all of MSA's requirements had been met. The three-piece power generation system (pneumatic motor, reversed DC motor, and accumulator) successfully produced an acceptable amount of power from the air flow initiated by the human breathing cycle while harboring no undesirable side effects and requiring no changes to the current SCBA design. The design of the air-driven generator, however, had been centered around the need for performance testing and was not suited for commercial production. Optimally, a commercially available power generator design would be small, lightweight, and easily added or removed from the system. This concept led to a necessary redesign of the assembly.

In the wake of the majority of performance testing, there remained a few concerns about the generation system's potential to be commercially produced. The assembly of components, as it stood, was bulky, awkward, and exceeded a desirable weight for firefighters' use. Also, it had been noted that the pneumatic motor was leaking air around its rotating shaft which meant wasting precious air and, consequently, shortening tank life. The combination of these issues led to a large change in the design of the components' assembly. It was conceived that the pneumatic and DC motors could be placed inside of the accumulator, possibly resolving both the issue of air leakage and that of the size and mobility of the power generator assembly, and putting to rest concerns regarding the maintenance of existing standards for air cylinder life.

Realizing the definite need for a compact and manageable final product, it was decided that size would drive the initial commercial design of the prototype power cell, and mask pressure issues would be resolved (if necessary) after its creation. Based on the dimensions of the Maxon DC motor and the Micromotors pneumatic motor, an initial design of the outer case of the power cell (which would act as the accumulator) was established. Anodized aluminum was chosen as a material because of its light weight, durability, and strength, as it would be acting as a pressure vessel. The new accumulator was machined, and its total volume was approximately 543 cm^3 with no apparatus inside. Recognizing that this volume was lower than the optimal 1338 cm^3 target value found through testing, three ports were machined into the walls of the outer case to allow for volume adjustment with regards to future mask pressure regulation.

To accommodate the alignment of the dynamo with its pneumatic counterpart within the accumulator, a mounting base was designed. The base was manufactured from 6061T651 aluminum and designed to be held in place within the outer case by two integral seal screws. The mounting support was adapted to accept both the interfaces of the dynamo and of the pneumatic motor and would keep both motors aligned while the coupling transmitted torque between them.

Because the air motor would now be enclosed within the accumulator, air leakage from any point would be considered unimportant since the air would be emitted within the accumulator either way. In fact, the exhausted air of the turbine would inherently cool the generator and any other electronics within the accumulator potentially allowing for a longer service life and a lower chance of equipment malfunction. For these reasons, a non-reversible air motor was considered an attractive option. The Micromotors MMF-0700 non-reversible air

motor was purchased for the prototype. This pneumatic motor, unlike its MMR-0700 counterpart, has only a single input for air and includes exhaust ports through which the air blows out, typically to atmosphere. (Technical data for the MMF-0700 can be found in the Appendix – Fig. (A.1-4).) The idea behind incorporating this non-reversible motor into the new accumulator design was that the used air would exhaust into the accumulator chamber, which would act as a reservoir for each breath the firefighter would take. As the accumulator's air supply would be depleted, the pressure drop would cause a new burst of air to flow into the chamber, generating power in the process. Also, it was believed that the new air motor would present less resistance to air flow, and therefore a possible increase in the output power. A simplified diagram of the inner workings of the power cell is shown below:

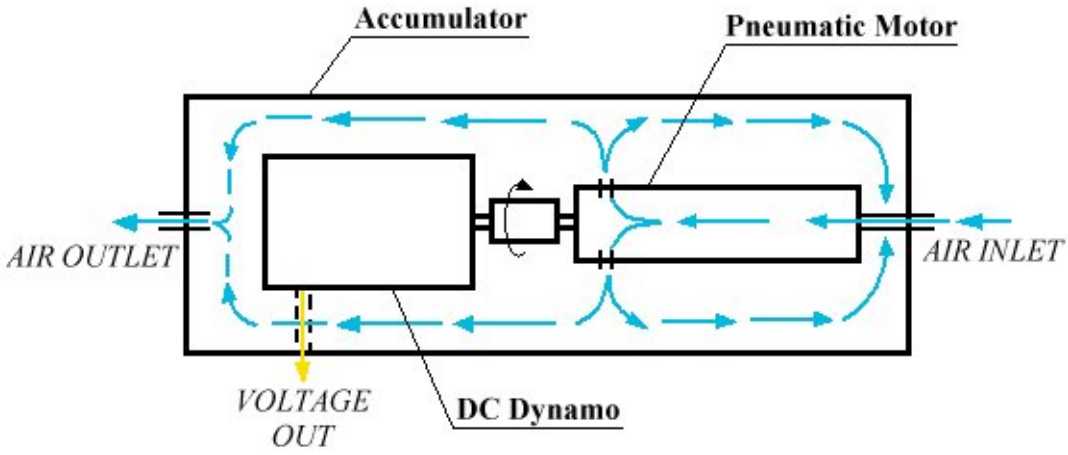

Figure 3.1: Dynamics of the New Power Cell Design

In addition to a redesign of the dynamics of the power cell assembly, multiple other improvements were made. An upgraded Berg custom-bored, six-beam flexible coupling (for between the DC and pneumatic motors) was used, replacing the solid aluminum coupling employed in performance testing. (The solid coupling had demonstrated problems associated with alignment and slip.) Head flanges were machined from 6061 BlackHardcoat anodized

aluminum for the ends of the power cell, and were each fixed with eight socket head cap screws. The flanges included Buna-N o-rings to seal the pressurized accumulator. Snap-Tite female and male connectors were affixed through the end caps, so that the unit could be easily added to or removed from the SCBA. Finally, a Pave Technology Feedthrough Connector was placed through the outer case and wired to the dynamometer in order to monitor the performance of the power cell with respect to the dynamo's rotational speed.

The figure below is a sectioned view illustrating the final design of the power generation cell assembly and all of its associated components:

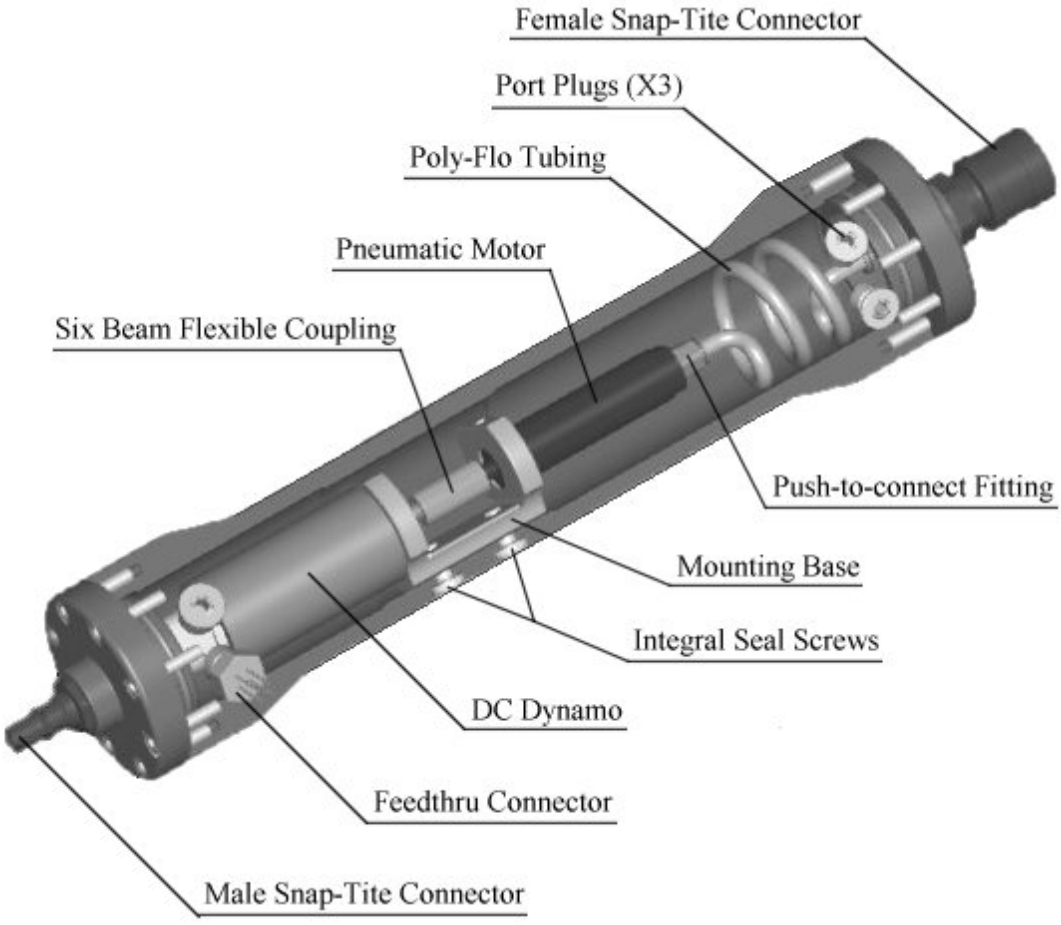

Figure 3.2: Power Cell Assembly

3.2 PRODUCT REQUIREMENT TESTING

After the appropriate parts had been machined and the final power cell product assembled, there existed a need to both test the generator for its capability in powering the SCBA's associated electrical components and to focus on any final points of optimization based on these tests. Initially, it was desirable to obtain some battery-operated device which could be powered by the generator, placing it under a realistic loading condition for testing purposes. An 18-LED emergency strobe light, typically requiring four AA batteries, was purchased. The batteries were removed and the light was hard wired to generators electrical output. The power cell was then connected to the NFPA breathing machine which was set to its lowest breathing rate. Preliminary testing proved successful, as the power cell easily lit up the emergency light, however, due to the pulsating nature of the power production, the light was not continuously on, but instead went out between the virtual breaths. This helped visualize a condition which had been assumed to be an obstacle to continuous power production all along. An electrical circuit would need to be created that provided the necessary capacitance to retain a sufficient charge during the "exhale" breaths such that the power cell would be, finally, producing a constant source of electrical power needed for the SCBA's electrical components.

While this electrical circuit was being contrived, it was decided that additional testing of the generation capabilities of the power cell be completed. This study included a comparison between the amount of power being generated and the pressure drop occurring across the pneumatic motor. Pressure gages were connected in sequence upstream of the cell and directly to the accumulator, and the electrical power generated was monitored. A constant pressurized flow of air was used, and the pressure drop was varied between 0 and 50 psig with an inline high-pressure regulator. The hope was that a certain optimal level (for power generation) of

input pressure could be found while gaining a greater understanding of the dynamic characteristics of the new power cell design. Tests were performed under both unloaded (generator powering nothing) and loaded (generator powering test light) conditions and the following results were obtained:

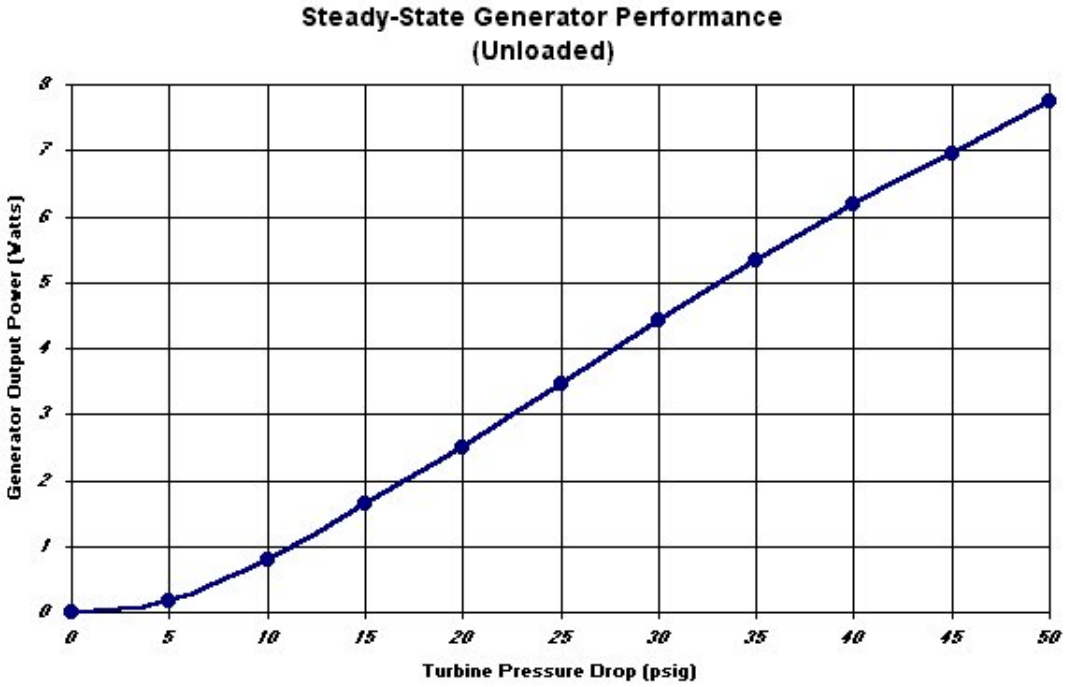

Figure 3.3: Power Cell Output vs. Turbine Pressure Drop – Unloaded State

Running the generator test in the unloaded state produced a very linear trend between the pressure drop across the turbine and the electrical power produced by the generator. The difference in pressure transversely over the pneumatic motor was limited to less than 50 psig, as the second-stage regulator was not designed to handle lower input pressures. With no load present in the system, these results seemed reasonable and showed no evident limitations associated with the dynamics of the system.

An identical test was performed with the power cell connected to the 18-LED emergency light in order to add what could be considered a realistic operating load to the system. The following graph depicts the dynamic trend of the power production under this electrical load:

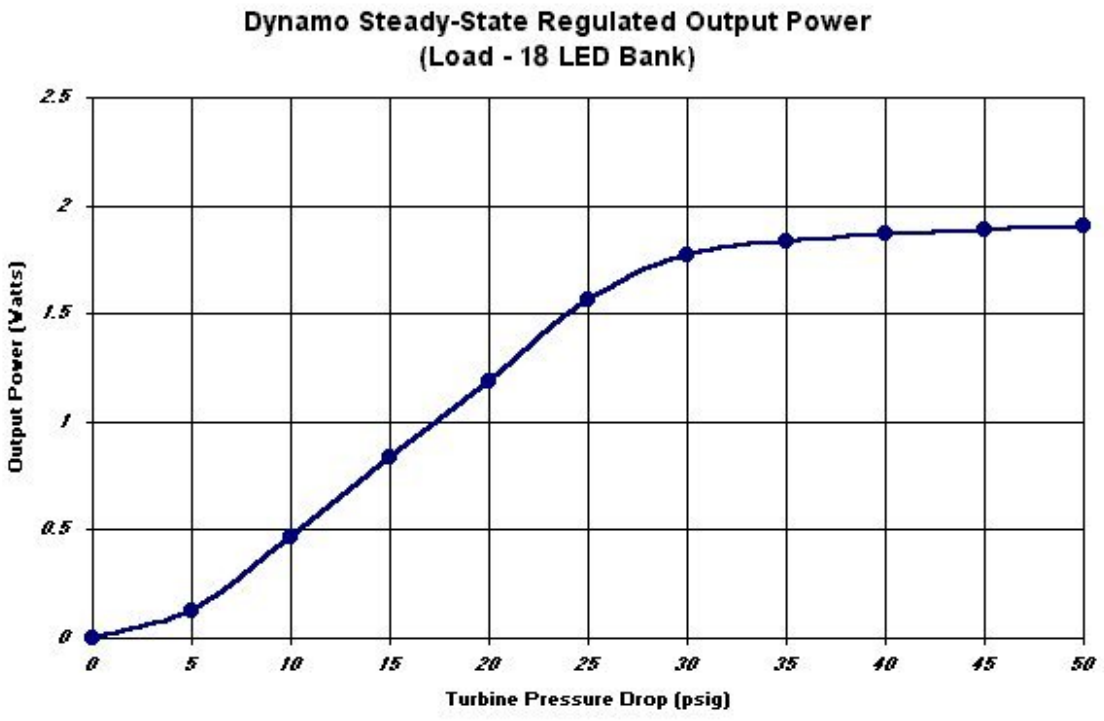

Figure 3.4: Power Cell Output vs. Turbine Pressure Drop – Loaded State

When powering the emergency light, the power cell is seen to have different output power characteristics with regards to pressure drop than seen previously. In this case, the output power levels off just under 2 Watts. This test shows that the efficiency of the generator's performance is highly dependent on the electrical composition of the device being powered.

For the purposes of justifying realistic commercial use of the power cell design, these tests were not adequate. First, the electrical power had to be provided in constant form, such that any of the SCBA's related electrical components could be continuously powered both during the

inhalation and exhalation portions of the human breathing cycle. Secondly, the power cell prototype would then have to be tested for its ability to operate these components uninterruptedly over a period of time. To ensure a source of continuous power delivery, an electrical circuit was constructed which included the capacitance necessary to store the charge generated by the power cell long enough to supply a device with electrical power over the inactive exhalation portion of the breathing cycle.

The combination of the capacitance circuit wired to the power cell was used for testing various electrical components including several of MSA's existing firefighter devices. Connected with the NIOSH breathing simulation machine, the generator successfully powered the 18-LED emergency light, MSA's Dragonfly Personal Alert Safety System, the Evolution 5000 Thermal Imaging Camera, and an electronic communications device. All of these components had previously relied on DC batteries which had been removed and replaced with wiring to the power cell's output terminals.

Even with the achievements of these performance tests, there still existed one major obstacle to a completely successful project. Due to the reduced size of the outer case (accumulator) in the new power cell design to 543 cm^3 from the optimal volume discovered earlier to be approximately 1338 cm^3, mask pressure was once again dipping below atmospheric, a condition deemed unacceptable by NIOSH standards. Being that the pressure drop across the first-stage regulator (and therefore the input pressure to the power cell) was somewhat adjustable, and a major goal of the project was to avoid unnecessary redesign of existing SCBA components, testing was performed by adjusting the first-stage regulator in hopes of bringing the mask pressure back up into the acceptable positive pressure range necessary for the user's safety. This test yielded excellent results, whereby increasing the power cell's inlet pressure a mere 5-10

psi, the mask pressure was brought into positive atmospheric. A graph of mask pressure with respect to the first-stage regulator's adjusted outlet pressure is shown below in Fig. (3.5).

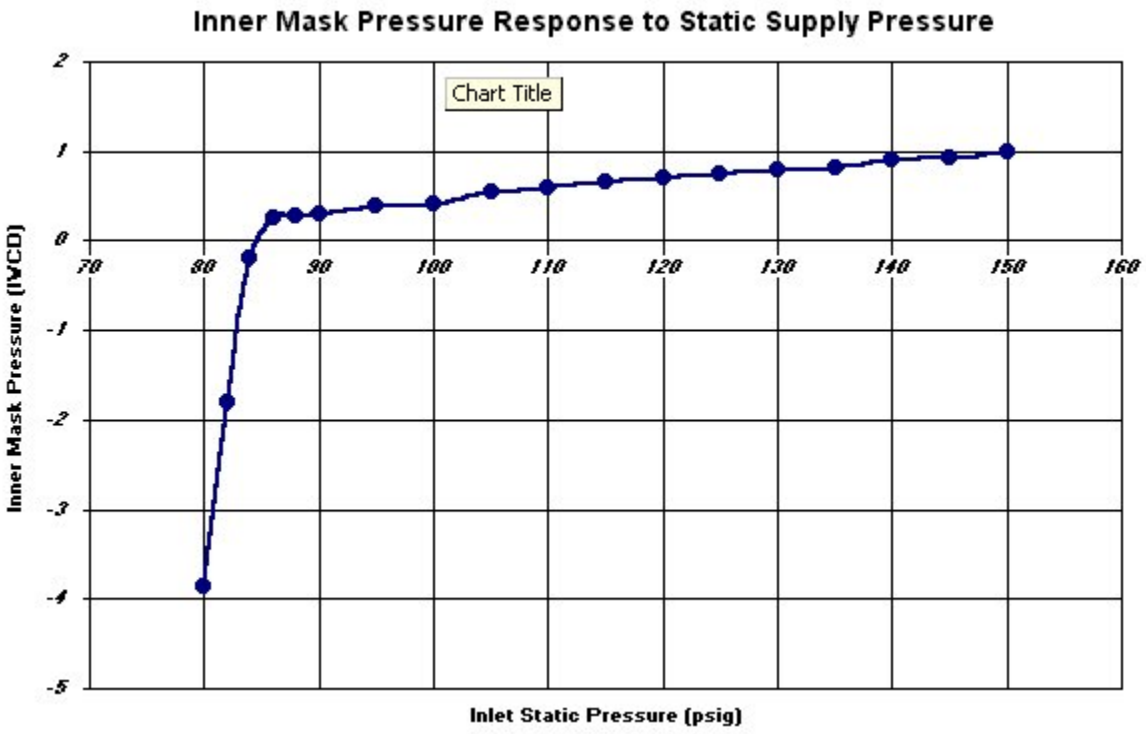

Figure 3.5: Inner Mask Pressure vs. Adjusted Power Cell Inlet Pressure

This simple adjustment of the first stage regulator is easy to perform and makes the mask pressure variance 100% NIOSH acceptable.

4.0 CONCLUSION

Upon the success of the first-stage regulator's outlet pressure adjustment, the power cell design had met or surpassed all of MSA's requirements for an SCBA-integrated energy harvesting device. Testing ensued in which the breathing machine was replaced by an actual user, and the results were consistent with those previously obtained. (See Fig. (B.7-8) in the Appendix for photographs of the fully functional SCBA with integrated power cell). It should be noted that before the power cell were to reach a level of public use, certain conditions would most likely have to be provided for in the design to ensure the safety of the user. Most prominently, a bypass valve should be placed in line such that if, for some reason, the flow of air was blocked within the power cell, a valve would switch, bypassing the unit and allowing the user to breath freely once again (with no power generation).

Research showed that no similar power generation device exists, as certain characteristics of the power cell design set it apart from all other present technologies. The generator's uniqueness is demonstrated in a variety of ways. No external source of energy is required for the power cell's use or maintenance, as the air that drives the pneumatic motor (and in turn the power-producing dynamo) is being used in its entirety as a breathing supplement for the firefighter. Therefore, nothing except previously-wasted potential energy is sacrificed with the power cell's implementation. Furthermore, having the accumulator completely encompass the mechanical and electrical components used for power generation offers a protective enclosure as

well as an overall compact design. This design also provides the dynamo with a consistent supply of turbulent air for cooling purposes.

Because of such exclusive attributes of the power cell, and because the potential for commercial success is decidedly high, plans are in place for the acquisition of a U.S. patent. Although there remain some marketing investigations and feasibility studies to be done, the power generation research has proven itself a success from the standpoints of both research and commercialized industry.

APPENDIX A

Technical Data and Additional Diagrams

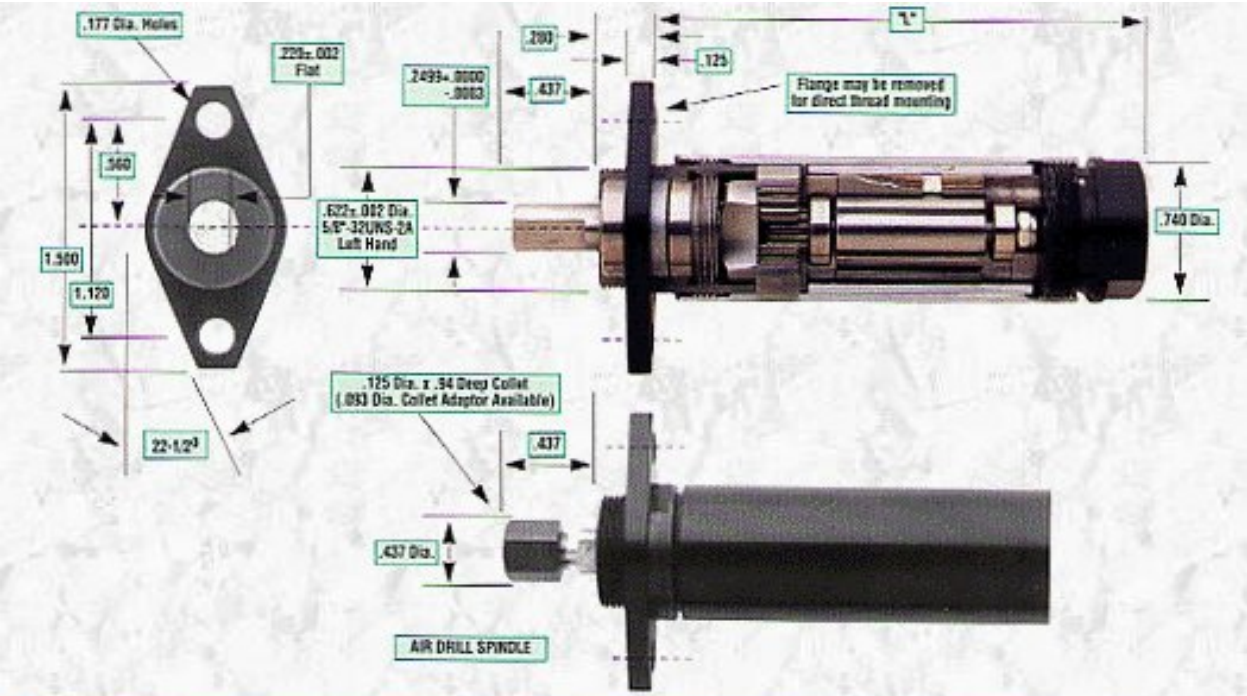

AIR DRILL		AIR MOTOR		FREE SPEED	STALL TORQUE INCH OUNCES	"L" LENGTH INCHES	APPROXIMATE WEIGHT:OUNCES
RIGHT HAND	REVERSIBLE	RIGHT HAND	REVERSIBLE				
MMD-5000	MMDR-5000	MMF-5000	MMR-5000	50,000	3.5	2.56	3-1/4
MMD-2800	MMDR-2800	MMF-2800	MMR-2800	28,000	7.2	2.56	3-1/4
MMD-0700	MMDR-0700	MMF-0700	MMR-0700	7,000	24	2.56	3-1/4
MMD-0014	MMDR-0014	MMF-0014	MMR-0014	1,750**	110	3.19	4-1/4
MMD-0004	MMDR-0004	MMF-0004	MMR-0004	450**	440	3.81	4-3/4
+	+	MMF-0002	MMR-0002	225**	850	3.81	4-3/4
+	+	MMF-0001	MMR-0001	110**	1750	4.44	5-1/2
+	+	MMF-5001	MMR-5001	28**	1750*	5.06	6-1/2
+	+	MMF-6001	MMR-6001	7**	1750*	5.69	7

Figure A.1: Pneumatic Motor Technical Drawings and Information

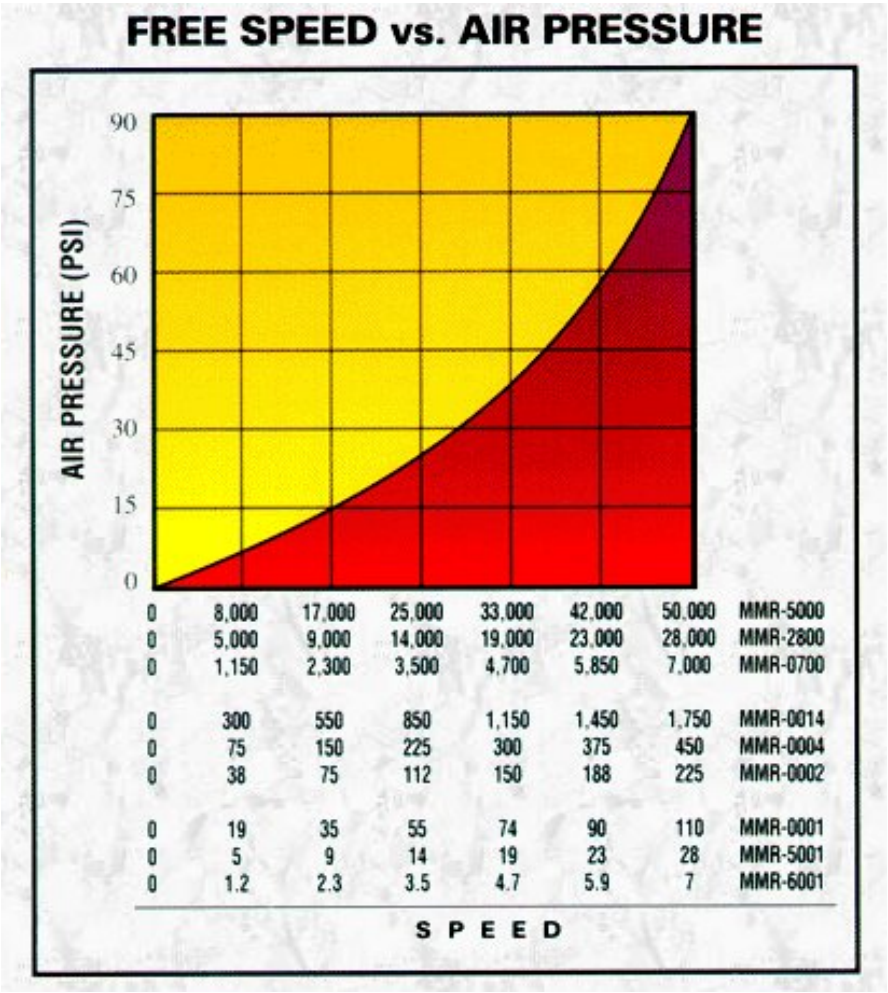

Figure A.2: Pneumatic Motor Technical Data – FREE SPEED vs. AIR PRESSURE

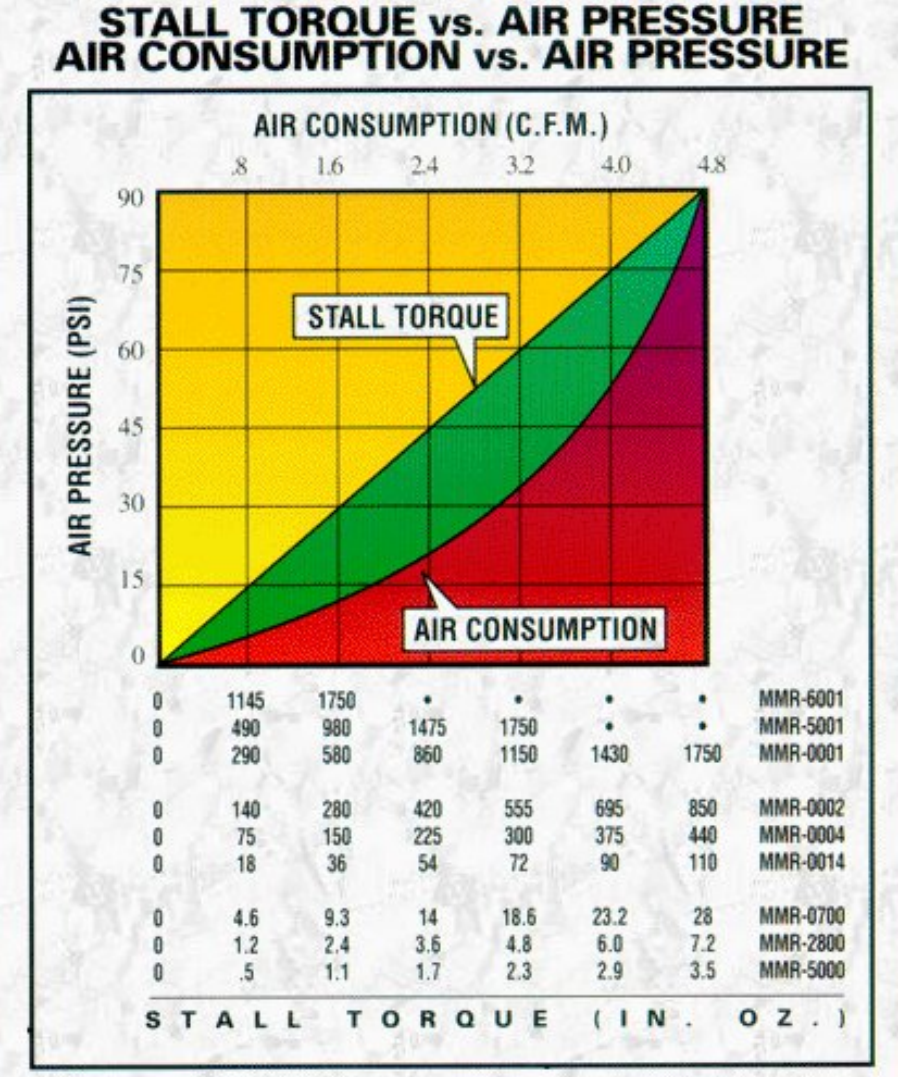

Figure A.3: Pneumatic Motor Technical Data – AIR CONSUMPTION vs. AIR PRESSURE

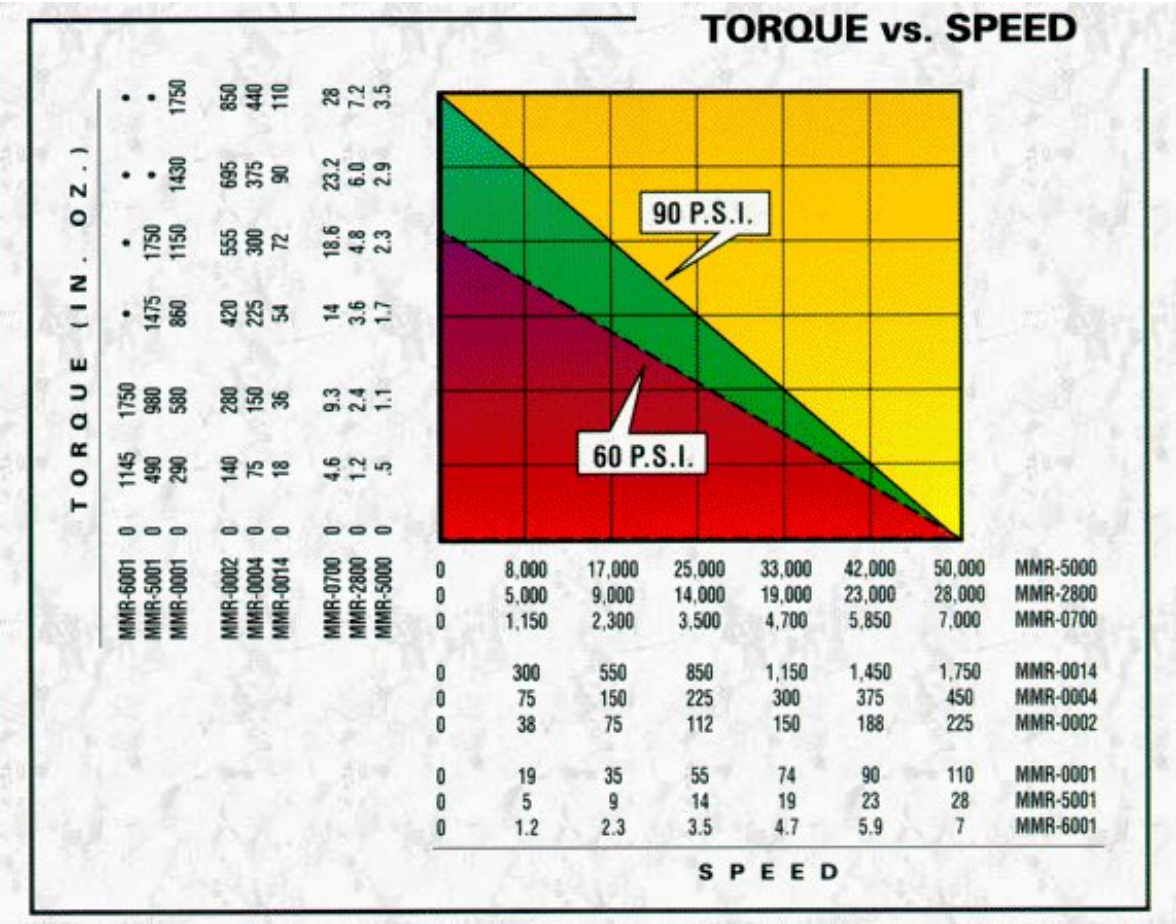

Figure A.4: Pneumatic Motor Technical Data – TORQUE vs. SPEED

maxon DC motor

RE 35 ∅35 mm, Graphite Brushes, 90 Watt

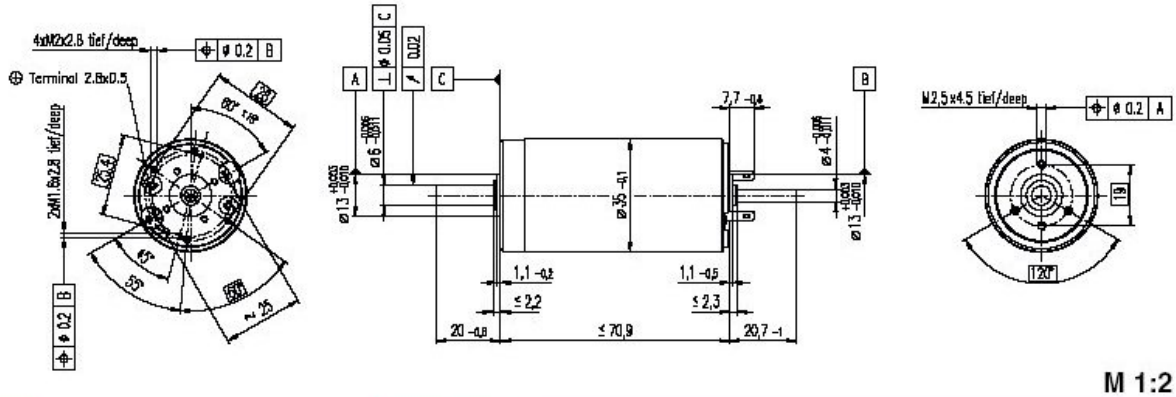

M 1:2

Stock program
Standard program
Special program (on request!)

			Order Number														
			118776	118777	118778	118779	118780	118781	118782	118783	118784	118785	118786	118787	118788	118789	118790
Motor Data																	
1	Assigned power rating	W	90	90	90	90	90	90	90	90	90	90	90	90	90	90	90
2	Nominal voltage	Volt	15.0	30.0	42.0	48.0	48.0	48.0	48.0	48.0	48.0	48.0	48.0	48.0	48.0	48.0	48.0
3	No load speed	rpm	7070	7220	7530	7270	6650	5970	4750	3810	3140	2570	2100	1620	1290	1060	856
4	Stall torque	mNm	872	949	1070	966	878	766	613	493	394	320	253	194	155	125	99.5
5	Speed / torque gradient	rpm / mNm	8.45	7.77	7.17	7.63	7.68	7.89	7.86	7.84	8.09	8.19	8.47	8.55	8.54	8.80	8.94
6	No load current	mA	245	124	93	77	69	60	45	34	27	22	17	13	10	8	7
7	Starting current	A	44.9	24.4	20.3	15.5	12.9	10.1	6.43	4.16	2.74	1.83	1.18	0.704	0.448	0.298	0.193
8	Terminal resistance	Ohm	0.334	1.23	2.07	3.09	3.72	4.75	7.46	11.5	17.5	26.2	40.5	68.2	107	161	248
9	Max. permissible speed	rpm	8200	8200	8200	8200	8200	8200	8200	8200	8200	8200	8200	8200	8200	8200	8200
10	Max. continuous current	A	4.00	2.74	2.15	1.78	1.63	1.45	1.17	0.944	0.768	0.630	0.508	0.392	0.313	0.256	0.206
11	Max. continuous torque	mNm	77.7	107	113	111	111	110	111	112	111	110	109	108	108	107	106
12	Max. power output at nominal voltage	W	152	175	206	181	150	118	75.0	48.4	31.8	21.2	13.7	8.07	5.10	3.36	2.15
13	Max. efficiency	%	81	84	86	85	85	84	83	82	80	79	77	74	72	69	66
14	Torque constant	mNm / A	19.4	38.9	52.5	62.2	68.0	75.8	95.2	119	144	175	214	276	346	418	515
15	Speed constant	rpm / V	491	246	182	154	140	126	100.0	80.6	66.4	54.6	44.7	34.6	27.6	22.9	18.5
16	Mechanical time constant	ms	6	5	5	5	5	5	5	5	5	5	5	5	5	5	5
17	Rotor inertia	gcm²	65.5	65.5	69.6	65.0	64.5	62.7	62.8	62.8	60.7	59.9	57.9	57.2	57.2	55.5	54.5
18	Terminal inductance	mH	0.09	0.34	0.62	0.87	1.04	1.29	2.04	3.16	4.65	6.89	10.30	17.10	26.90	39.30	59.70
19	Thermal resistance housing-ambient	K / W	6.2	6.2	6.2	6.2	6.2	6.2	6.2	6.2	6.2	6.2	6.2	6.2	6.2	6.2	6.2
20	Thermal resistance rotor-housing	K / W	2.0	2.0	2.0	2.0	2.0	2.0	2.0	2.0	2.0	2.0	2.0	2.0	2.0	2.0	2.0
21	Thermal time constant winding	s	27	27	29	27	27	26	26	26	25	25	24	24	24	23	23

Figure A.5: RE 35 DC Motor Technical Drawings and Information

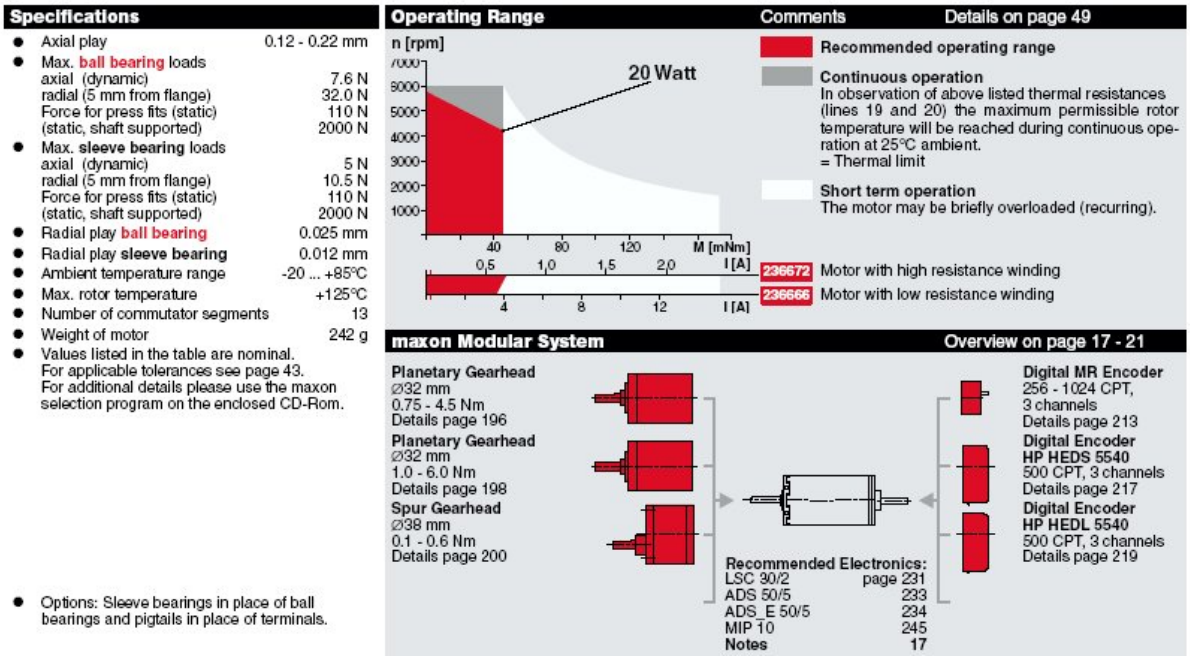

Figure A.6: RE 35 DC Motor – Additional Information

maxon A-max

A-max 32 ∅32 mm, Graphite Brushes, 20 Watt

HighPower

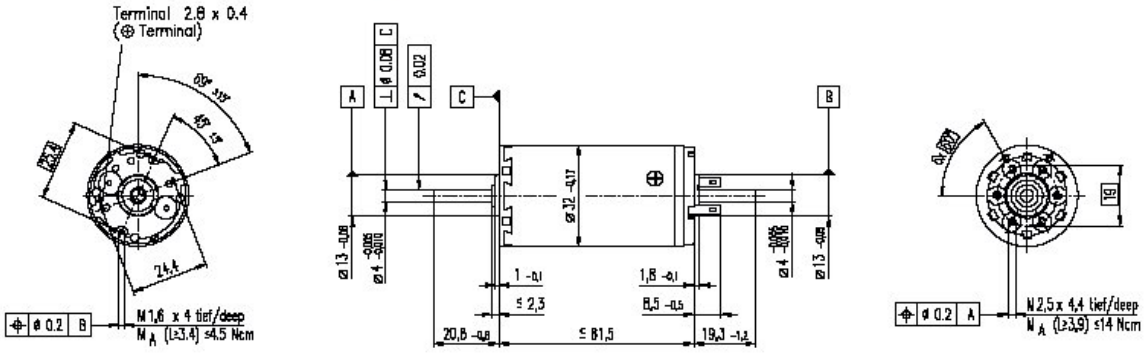

M 1:2

Stock program
Standard program
Special program (on request!)

			Order Number						
			236666	236667	236668	236669	236670	236671	236672
Motor Data									
1	Assigned power rating	W	20	20	20	20	20	20	20
2	Nominal voltage	Volt	6.0	9.0	12.0	24.0	30.0	36.0	42.0
3	No load speed	rpm	4780	4920	4610	6420	6130	5820	5620
4	Stall torque	mNm	121	130	131	206	194	187	178
5	Speed / torque gradient	rpm / mNm	41.0	39.0	36.0	31.7	32.1	31.6	32.1
6	No load current	mA	242	165	115	81	62	49	40
7	Starting current	mA	10500	7670	5430	5860	4220	3220	2530
8	Terminal resistance	Ohm	0.573	1.17	2.21	4.09	7.11	11.2	16.6
9	Max. permissible speed	rpm	6000	6000	6000	6000	6000	6000	6000
10	Max. continuous current	mA	3610	2520	1840	1350	1020	817	671
11	Max. continuous torque	mNm	41.7	42.7	44.5	47.3	47.1	47.5	47.1
12	Max. power output at nominal voltage	mW	14100	16000	15300	33900	30500	28000	25700
13	Max. efficiency	%	69	71	72	77	77	77	76
14	Torque constant	mNm / A	11.5	17.0	24.2	35.1	46.0	58.1	70.2
15	Speed constant	rpm / V	827	563	394	272	208	164	136
16	Mechanical time constant	ms	18	16	15	14	14	14	14
17	Rotor inertia	gcm²	42.4	39.0	39.7	43.0	41.9	42.2	41.3
18	Terminal inductance	mH	0.06	0.13	0.26	0.55	0.95	1.52	2.21
19	Thermal resistance housing-ambient	K / W	7.5	7.5	7.5	7.5	7.5	7.5	7.5
20	Thermal resistance rotor-housing	K / W	2.1	2.1	2.1	2.1	2.1	2.1	2.1
21	Thermal time constant winding	s	17	16	16	17	17	17	17

Figure A.7: A-max 32 DC Motor Technical Drawings and Information

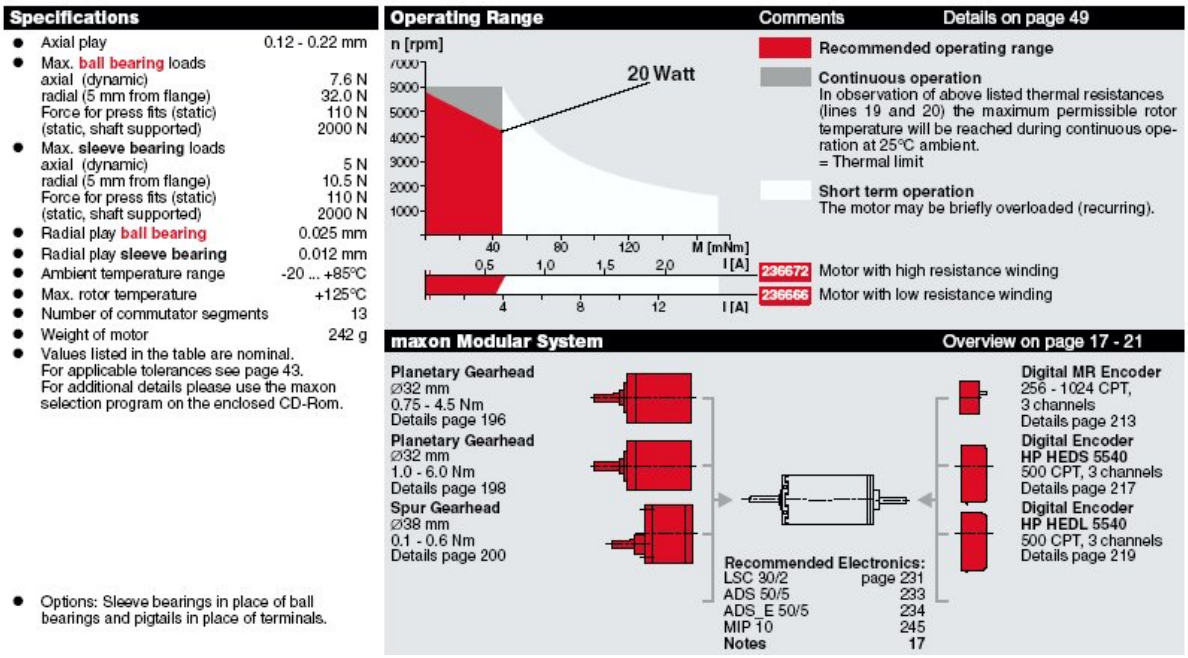

Figure A.8: A-max 32 DC Motor – Additional Information

ARO

0000 - Series Power Motors

MODEL	SPINDLE	R.P.M. FREE SPEED	R.P.M. LOAD SPEED @MAX. H.P.	TORQUE STALL lb. ft.	TORQUE STALL Nm	TORQUE OUTPUT @MAX. H.P. lb. ft.	TORQUE OUTPUT @MAX. H.P. Nm	AIR CONSUMPTION @FREE SPEED CFM	AIR CONSUMPTION @FREE SPEED L/s	SOUND LEVEL @FREE SPEED dB(A)	WEIGHT lbs.	WEIGHT kg.	GEAR REDUCTION
FORWARD ROTATION - .10 H.P.													
8610-A	3/8" Keyed	1,000	500	1.8	2.4	1.05	1.4	9.5	4.5	80	90	.40	Double
8611-A	3/8" Keyed	5,000	2,500	.42	.6	.21	.3	9.5	4.5	80	80	.36	Single
8616-A	3/8"-24 Th'd.	1,000	500	1.8	2.4	1.05	1.4	9.5	4.5	80	.90	.40	Double
8617-A	3/8"-24 Th'd.	5,000	2,500	.42	.6	.21	.3	9.5	4.5	80	.80	.36	Single
8618-A	3/8"-24 Th'd.	25,000	13,000	.10	.1	.04	.05	9.5	4.5	80	.80	.36	Single
REVERSIBLE - .10 H.P.													
8613-A	3/8" Keyed	1,000	500	1.8	2.6	1.05	1.4	11.5	5.4	80*	.90	.40	Double
8614-A	3/8" Keyed	5,000	2,500	.42	.6	.21	.3	11.5	5.4	80*	.80	.36	Single

*Requires installation for reversible motors - shown on page 30.

Figure A.9: Manufacturer Data for ARO 8416-A Pneumatic Motor

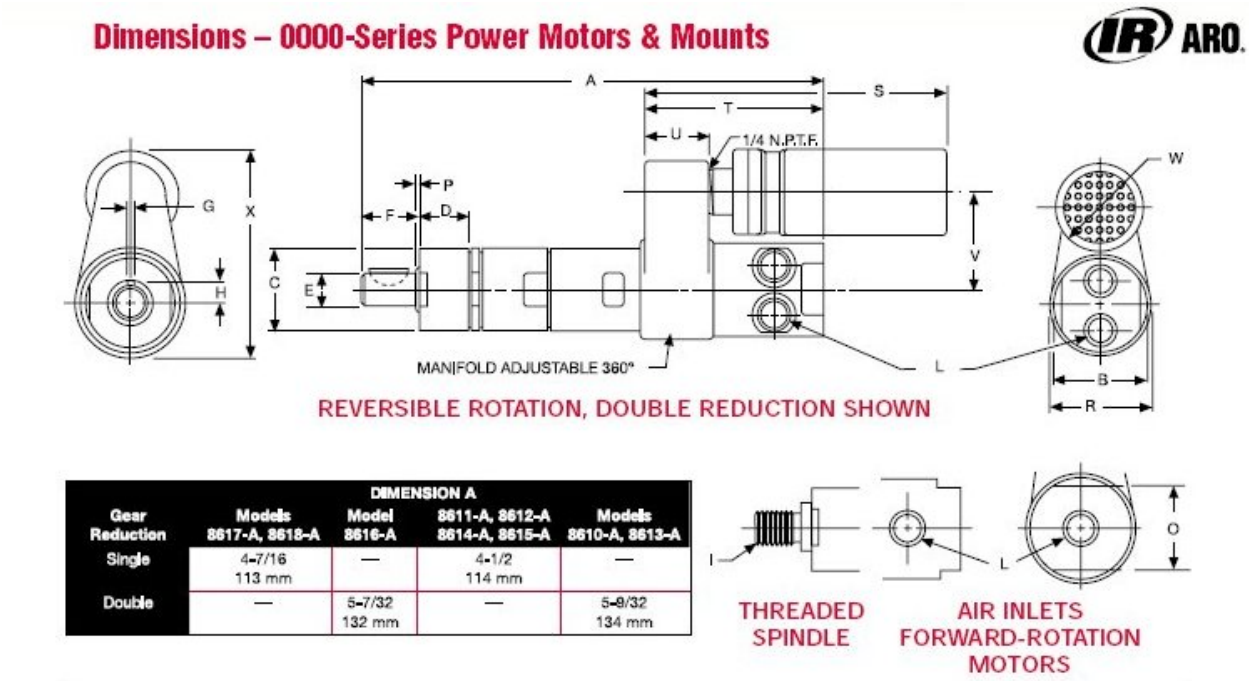

Gear Reduction	DIMENSION A Models 8617-A, 8618-A	Model 8616-A	8611-A, 8612-A 8614-A, 8615-A	Models 8610-A, 8613-A
Single	4-7/16 113 mm	—	4-1/2 114 mm	—
Double	—	5-7/32 132 mm	—	5-9/32 134 mm

Scale	B	C	D	E	F-Keyed Spindle	F-Th'd. Spindle	G	H	I	L	O
Inches	1-1/16	.936 .937	.580 .590	.374 .375	.644 .691	.581 .628	.0938 .0948	.228 .238	3/8"-24 UNF-2A	1/8 NPTF	7/8
mm	27	23.77 23.80	14.73 14.99	9.50 9.53	16.36 17.55	14.76 15.95	2.38 2.41	5.79 6.05	Th'd.	Air Inlet	22

Scale	S P-Keyed Spindle	P-Th'd Spindle	R	Reversible Direction	Single Direction	T	U	V	W	X
Inches	.149 .186	.024 .061	1-1/8	3-7/16	4-7/16	2-1/32	3/4	1-1/8	1	2-3/16
mm	3.78 4.72	.61 1.55	28	87 mm	113 mm	51	19	28	25	55

Figure A.10: ARO 8416-A Pneumatic Motor Technical Drawings and Information

APPENDIX B

Miscellaneous Additional Information

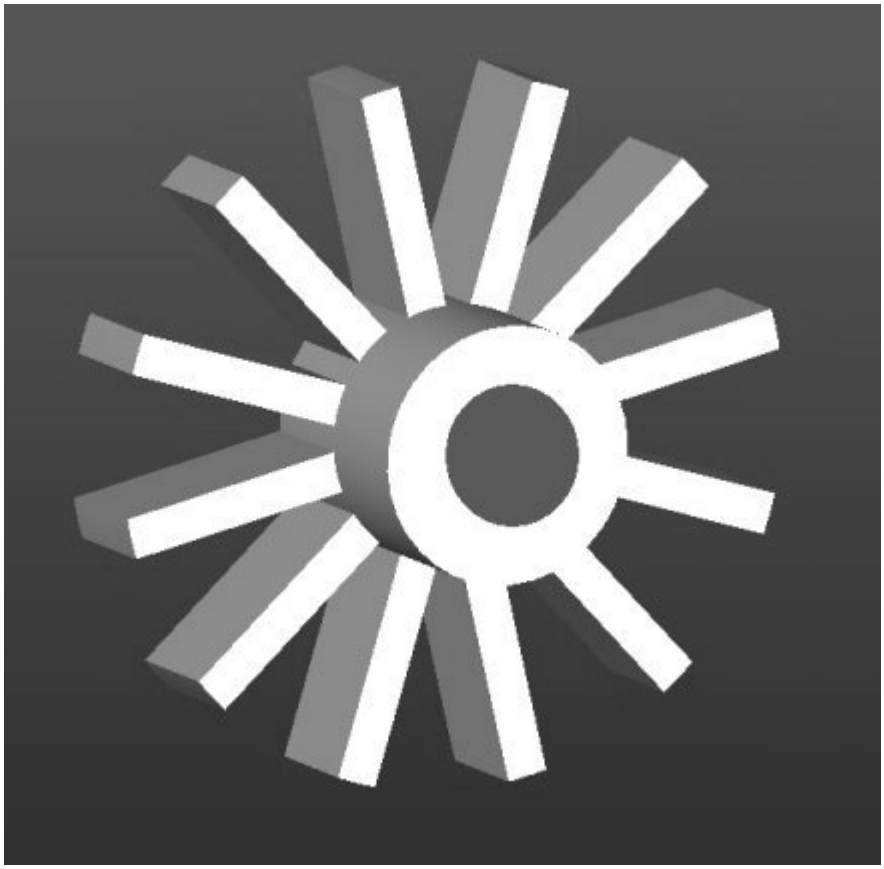

Figure B.1: Impulse Paddle Wheel Turbine Design

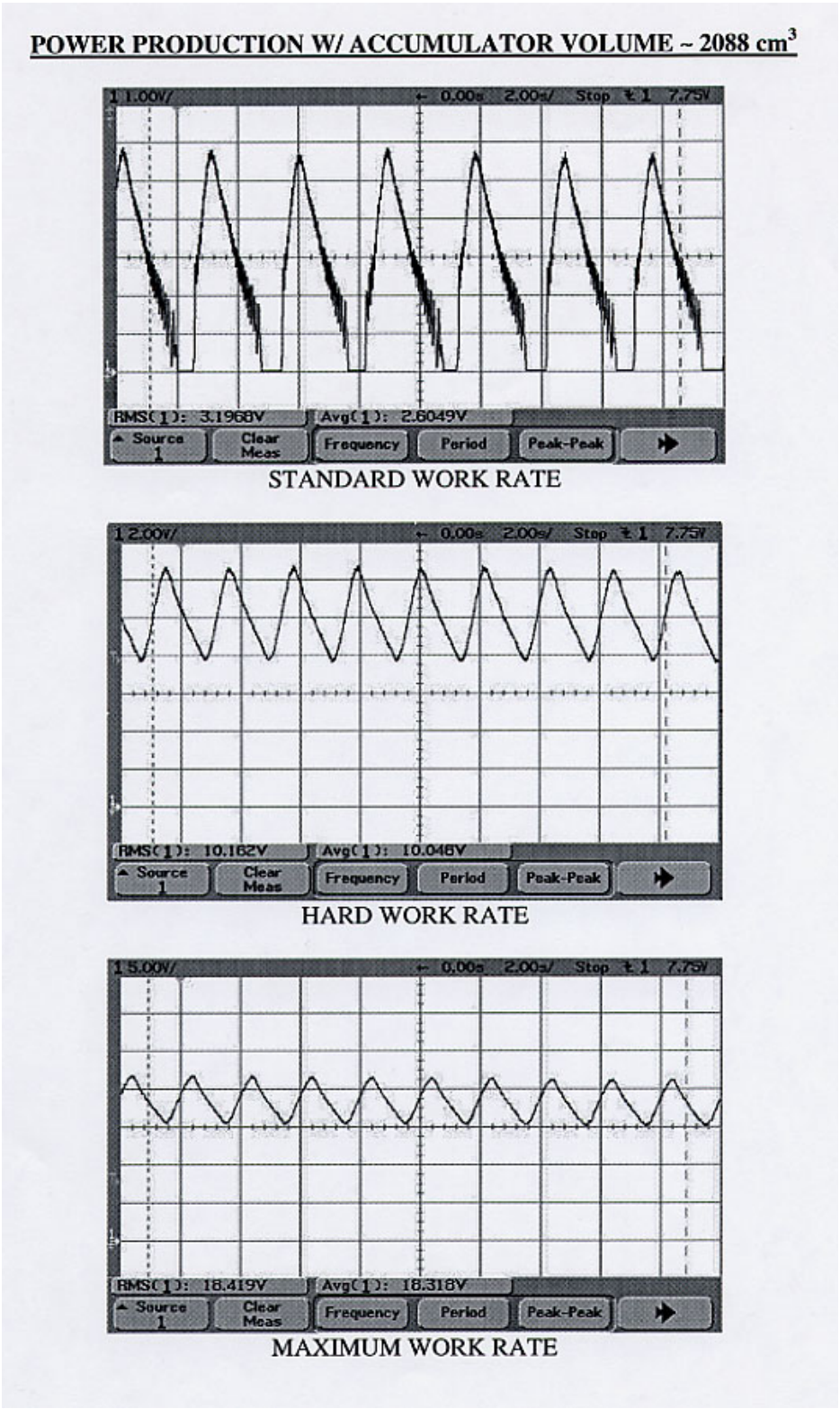

Figure B.2: Power Output Behavior for 2088 cm^3 Accumulator Volume

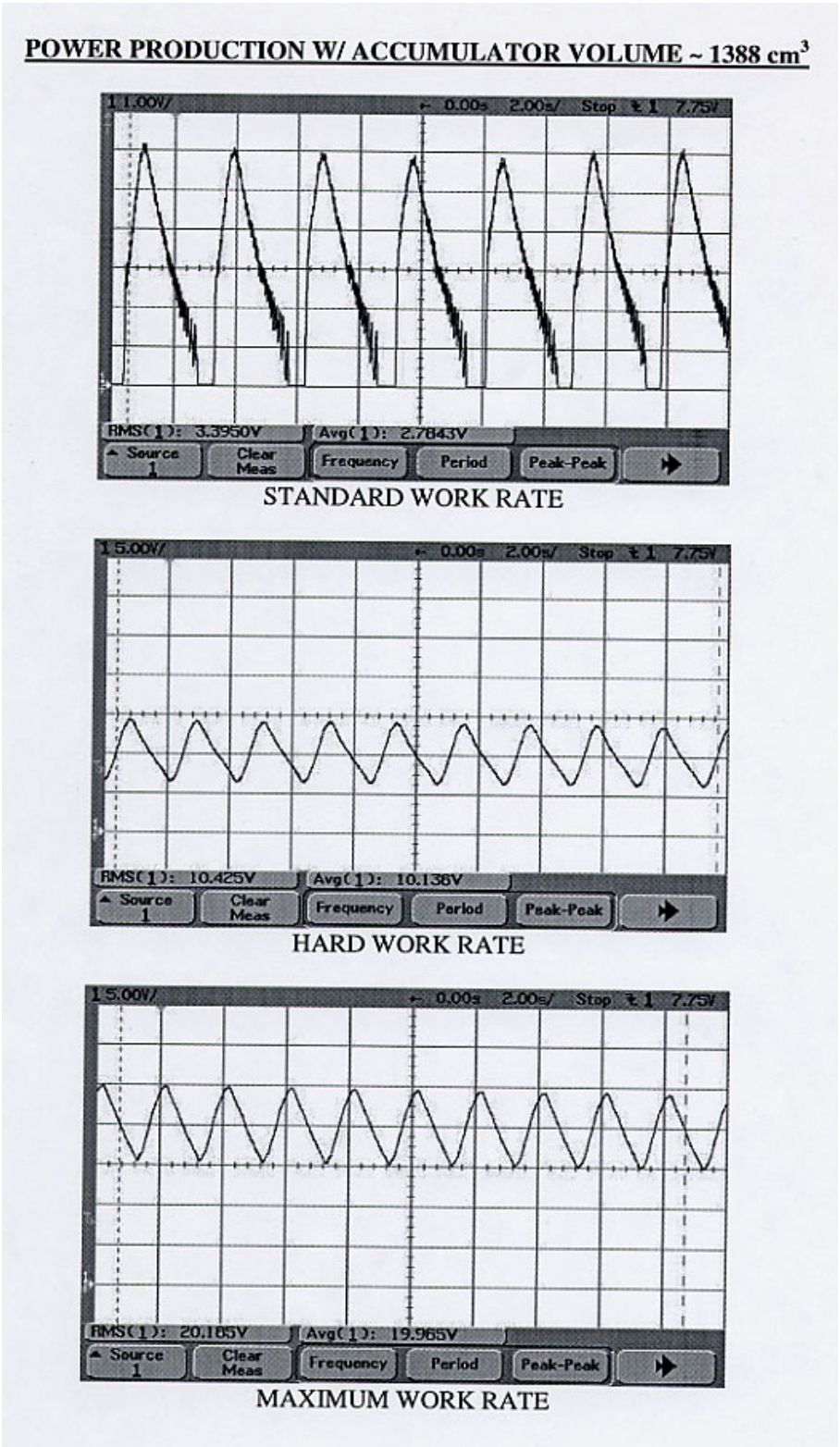

Figure B.3: Power Output Behavior for 1388 cm^3 Accumulator Volume

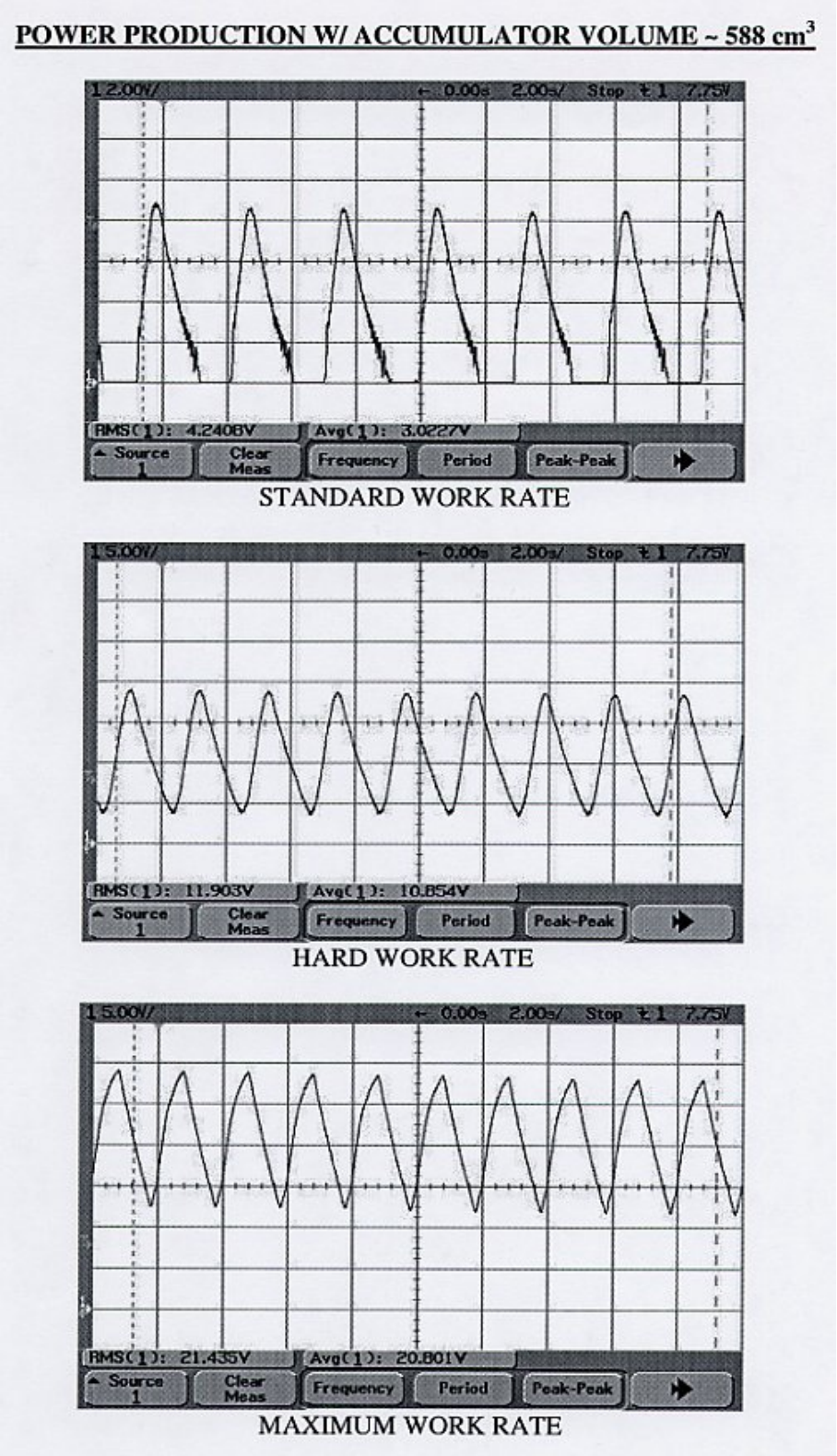

Figure B.4: Power Output Behavior for 588 cm^3 Accumulator Volume

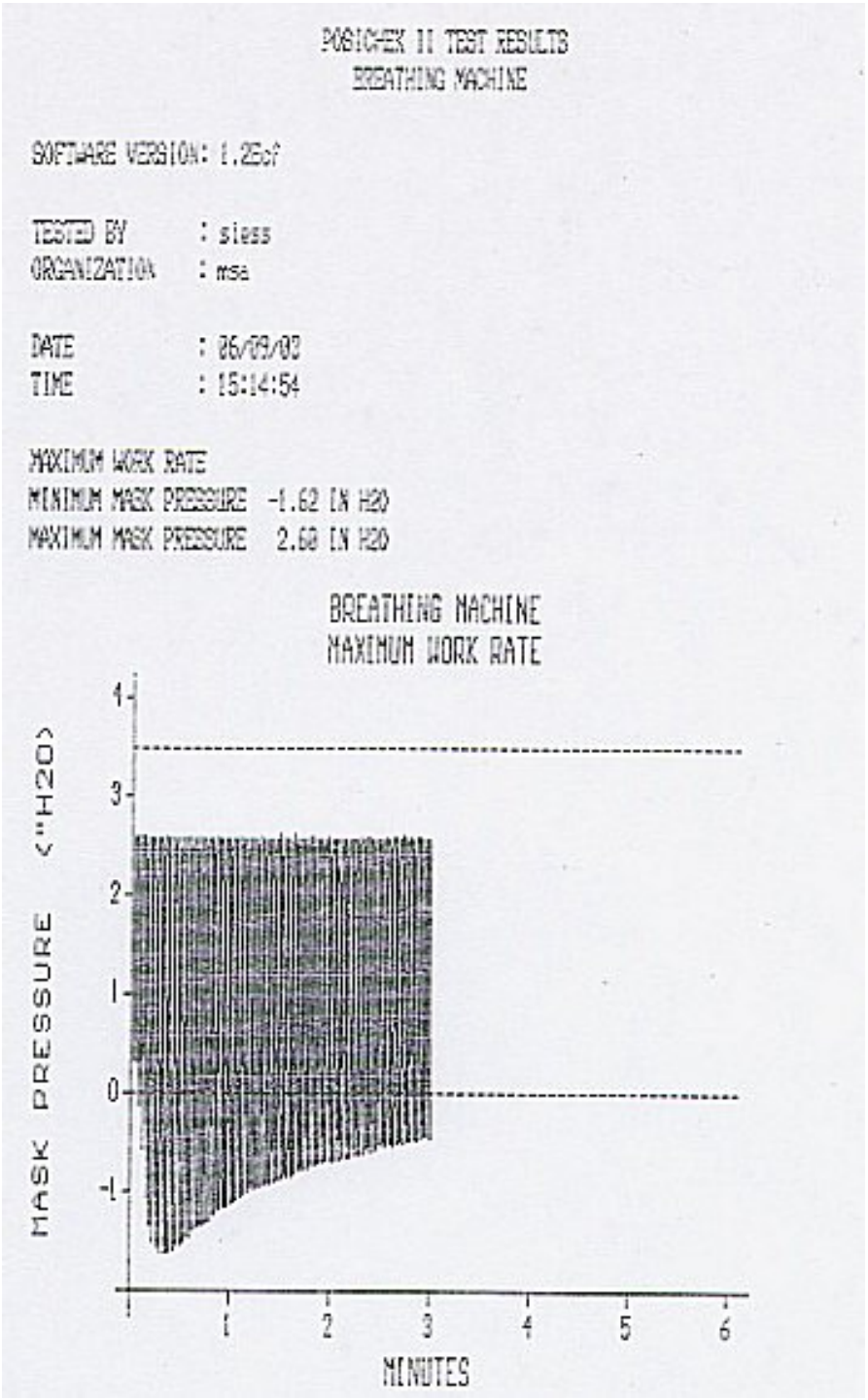

Figure B.5: Phenomena of Mask Pressure Striving for Dynamic Equilibrium

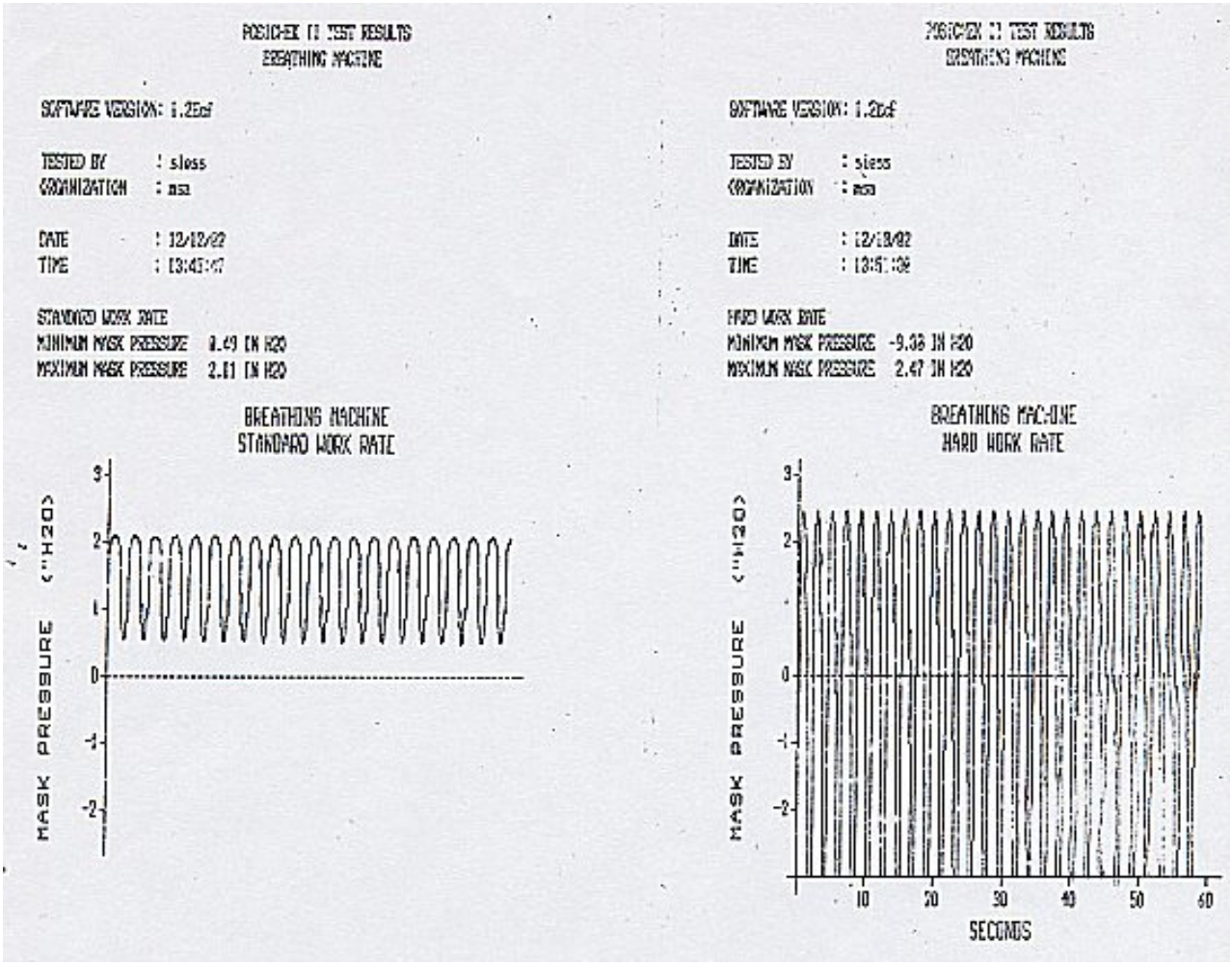

Figure B.6: Mask Pressure Dropping Below Zero at NIOSH Maximum Breathing Rate

Figure B.7: Photograph of Final Power Cell Prototype

Figure B.8: Photograph of Implementation of Functional Power Cell

BIBLIOGRAPHY

1. Cengel, Y. A., *Introduction to Thermodynamics and Heat Transfer*, McGraw-Hill, 1997. Ch. 2, 58-59.

2. *Fuel Cell Basics*, Fuel Cell Test and Evaluation Center, Concurrent Technologies Corporation, 14 March 2004. <http://www.fctec.com/fctec_types_pem.asp>

3. Albanyan, O., Belasco, D., and Schlabach, M, *Conceptual Design of a Piezoelectric Pressure Sensor and Display*, University of Pittsburgh, 1999.

4. Zawadzki, T., and Riegel, G., *Power Generation from a Pressurized Air Flow*, University of Pittsburgh, 2000.

5. Patrick, D., and Fardo, S., *Electricity and Electronics – A Survey*, Prentice-Hall, 1999. Ch. 5, 147-163.